Quaternary Science Reviews 29 (2010) 3468–3488

Contents lists available at ScienceDirect

Quaternary Science Reviews

journal homepage: www.elsevier.com/locate/quascirev

Holocene paleoceanography of the northwest passage, Canadian Arctic Archipelago

David Ledu [a,*], André Rochon [a,1], Anne de Vernal [b,2], Guillaume St-Onge [a,3]

[a] ISMER-UQAR and GEOTOP, 310 Allée des Ursulines, Rimouski, QC G5L 3A1, Canada
[b] GEOTOP, Université du Québec à Montréal, Montréal, QC H3C 3P8, Canada

ARTICLE INFO

Article history:
Received 15 April 2009
Received in revised form
7 June 2010
Accepted 10 June 2010

ABSTRACT

A series of cores (box and piston) were collected at 2 key locations in Lancaster Sound (cores 2004-804-009 BC and PC) and Barrow Strait (cores 2005-804-004 BC and PC) in the Canadian Arctic Archipelago to document the evolution of sea-surface conditions in the main axis of the Northwest Passage during the Holocene time period. Reconstruction of sea-surface parameters (summer temperature and salinity, duration of sea-ice cover) were estimated based on transfer functions using dinoflagellate cyst assemblages as proxy indicators. The chronology of these cores is based on calibrated AMS-^{14}C dates, ^{210}Pb analyses, and correlations between paleomagnetic secular variations of the geomagnetic field and a predicted spherical harmonic model of the geomagnetic field (CALS7 K.2). Our age models for both cores indicate that 009 PC spans the last 11,100 cal BP, while 004 PC encompasses the last 10,800 cal BP. Calculated sedimentation rates are in the range of 43–140 cm/kyr for core 009 PC and 15–118 cm/kyr for core 004 PC, allowing for a millennial time scale resolution in each core. Our results indicate relatively harsh conditions in Lancaster Sound between 10,800 and 9000 cal BP (summer temperatures 2 °C cooler than at present), which we associate with the presence of active ice-streams in northernmost Baffin Bay and a weak West Greenland Current. This is followed by a warming trend (up to 3 °C higher than present) that took place between ~8500 and 5500 cal BP, which we associate with the Holocene thermal maximum and to a large scale atmospheric pattern such as the Arctic Oscillation operating at the millennial time scale. This is concomitant with an increase in the relative abundance of phototrophic dinoflagellate cyst taxa. A gradual cooling of sea-surface temperature and increased sea-ice follow this from 5500 cal BP until the modern period. In Barrow Strait, harsh sea-surface conditions prevailed from 11,100 to 5500 cal BP, with summer temperatures as low as 4 °C cooler than at present. The warming trend occurred later in this region (between 5500 and ~1000 cal BP), after which a gradual cooling is observed until the modern period. The apparent shift, or opposite warming trends, between Lancaster Sound and Barrow Strait after 5500 cal BP could be the result of a change in atmospheric circulation patterns related to a possible shift in the AO mode (from AO$^+$ to AO$^-$). Comparison of ice core δ^{18}O record from Devon Island ice cap and the reconstructed sea-surface temperature from core 009 PC suggests a strong atmospheric-oceanic coupling throughout the Holocene in this area.

1. Introduction

Several recent studies have documented important hydrographic changes in the Arctic Ocean over the past three decades. Satellite data since 1978 show that the annual average Arctic sea-ice extent has decreased by 2.7% per decade, with larger decrease of 7.4% per decade in summer (IPCC, 2007). A minimum in the Arctic sea-ice extent and area was reached in September 2007, which is ~38% less than the historical climatological average (Comiso et al., 2008). The diminution of ice extent was accompanied by strong thinning of the halocline (Steele and Boyd, 1998) and warming of the Atlantic layer, which lies at 200–800 m depth (Polyakov et al., 2004). Most of these changes have been attributed to the impact of the Arctic oscillation (AO, Thompson and Wallace, 1998), whose index is defined as the leading principal component of Northern Hemisphere sea-level pressure (SLP). The AO is characterized by an exchange of atmospheric air mass between the Arctic Ocean and the surrounding zonal ring centered at about

* Corresponding author. Tel.: +1 418 723 1986 1230; fax: +1 418 724 1842.
E-mail addresses: david.ledu@uqar.qc.ca (D. Ledu), andre_rochon@uqar.qc.ca (A. Rochon), devernal.anne@uqam.ca (A. de Vernal), guillaume_st-onge@uqar.qc.ca (G. St-Onge).
[1] Tel.: +418 723 1986 1742.
[2] Tel.: +514 987 3000 8599.
[3] Tel.: +418 723 1986 1741.

0277-3791/$ – see front matter © 2010 Elsevier Ltd. All rights reserved.
doi:10.1016/j.quascirev.2010.06.018

45°N. It exerts a dominant role in the wind strength and direction, thus modulating both the location of the transpolar drift (TPD) and the extent of the anticyclonic Beaufort Gyre (BG, Proshutinsky et al., 2002). These in turn, affect the sea-ice motion and thickness enhancing changes of both the freshwater circulation pattern and budget in the Arctic Ocean (Rigor et al., 2002). Atmospheric and oceanic variability in the Arctic on seasonal, interannual and decadal time scale associated with the AO are relatively well-established (Proshutinsky and Johnson, 1997; Johnson et al., 1999; Venegas and Mysak, 2000; Polyakov and Johnson, 2000; Polyakov et al., 2004; Dukhovskoy et al., 2004). Longer time series records are required to better understand the natural climate variability in the Arctic Ocean at centennial to millennial time scale. Understanding these lower frequencies may be important for predicting future climate changes. Based on marine records and model experiments, it has been shown that the early Holocene was marked by a more extensive sea-ice cover in the western Arctic than in the eastern, whereas the late Holocene was marked by the reverse trend (Vavrus and Harrison, 2003; Kaufman et al., 2004; Rochon et al., 2006; Fisher et al., 2006; de Vernal et al., 2008, 2009), suggesting a longitudinal climatic gradient. In modern conditions a shift of the AO index (from AO^+ to AO^-) creates such sea-ice dipole patterns.

The Canadian Arctic Archipelago (CAA), which represents ~20% of the total shelf area in the Arctic (Jakobsson, 2002, 2004) is ideally located to better understand the nature of this thermal gradient because it connects the western and the eastern part of the Arctic Ocean. Moreover, relatively high biogenic flux allows the use of well-preserved biological proxies for the reconstructions of past sea-surface conditions. Holocene climate reconstructions in the CAA have been mostly inferred from paleolimnological data based on chironomidae (Gajewski et al., 2005; Rolland et al., 2008), diatoms (Finkelstein and Gajewski, 2007, 2008; Podritske and Gajewski, 2007), pollen (Zabenskie and Gajewski, 2007) and varved sediments (Besonen et al., 2008). Qualitative Holocene sea-ice history was also reconstructed based on bowhead bones remains (Savelle et al., 2000; Dyke and England, 2003), driftwoods (Dyke et al., 1997) and the abundance of the IP_{25} biomarker (Vare et al., 2009). Quantitative sea-surface reconstructions are only available at the westernmost (Rochon et al., 2006; Schell et al., 2008) easternmost (Rochon et al., 2006; Ledu et al., 2008) and central part (Ledu et al., 2007, 2008) of the main axis of the Northwest Passage (hereinafter referred to as MANWP). Poor preservation of biogenic calcium carbonate and biogenic silica in High Arctic marine sediments make difficult the use of foraminifers or diatoms to reconstruct sea-surface conditions. In contrast organic-walled microfossils or palynomorphs, in particular the cyst of dinoflagellates (or dinocysts) are composed of highly resistant polymer called dinosporine (Kokinos et al., 1998) and are well-preserved in the sediments, allowing their use for the reconstruction of sea-surface parameters.

In order to better understand the nature of the climatic gradient and the natural climate variability in the Arctic during the Holocene, we have collected marine sediment cores during two ArcticNet oceanographic campaigns aboard CCGS Amundsen ice breaker in the summer 2004 in Lancaster Sound (cores 2004-804-009 PC and 2004-804-009 BC) and in the summer 2005 in Barrow Strait (cores 2005-804-004 PC and 2005-804-004 BC) at the easternmost and central part of the MANWP, respectively. These cores show well-preserved dinocyst assemblages, which were used in conjunction with the modern analogue technique (MAT) to reconstruct summer (August) sea-surface temperature (SSTs) and salinity (SSSs) as well as the duration of sea-ice cover over the Holocene.

2. Environmental setting

2.1. General water mass distribution and major currents in the Arctic Ocean

Typically, the Arctic Ocean contains three distinct water mass. A low density surface layer or Polar Mixed Layer (PML) occupying the upper ~50–100 m of the water column, which is underlayed by a cold halocline down to ~200–300 m depth. This halocline mostly originates from the inflow of Pacific water through the Bering Strait and from the Arctic river inputs. Summer and winter thermal exchanges at the surface produce two forms of Pacific water that constitute the upper and middle halocline (McLaughlin et al., 2004; Steele et al., 2004). Finally, the halocline insulates the PML from the Atlantic water, which can be subdivided in warm intermediate Atlantic layer lying between 200 and 500 m depth and cold bottom Atlantic water below 500 m depth. The Atlantic water enters the Arctic through the Norwegian Atlantic water Current (NwAC), which is the northernmost extension of the North Atlantic Current (NAC). The NwAC consists of two branches (Fig. 1). The Barents Sea branch (BSB) flows eastward through the Barents Sea and the Fram Strait branch (FSB), which forms the West Spitsbergen Current (WSC) flowing poleward through eastern Fram Strait. The WSC divides into the Svalbard branch (SB) flowing northeast and the Yermak branch (YB), flowing northward (Rudels et al., 1994; Jones, 2001).

Both the Fram Strait and the Barents Sea branches join in the vicinity of Saint Anna Trough and move eastward along the Eurasian continental slope (Golubeva and Platov, 2007). A strong cyclonic boundary current along the margin of the Ocean Basins enhances a cyclonically movement to this water before recirculation in form of cyclonic gyres within the Canada, Makarov and Nansen basins (Rudels et al., 1994; Jones, 2001). Finally, the Atlantic water exits the Arctic Ocean via Fram Strait through the East Greenland Current (EGC), which flows southward into the Greenland and Norwegian seas. The EGC transports recirculating Atlantic water and the surface/sub-surface polar mixed layer (PML) as well the ice exported from the Arctic Ocean (Woodgate et al., 1999; Rudels et al., 1999). As it flows through southwest Greenland, the EGC mixed with the warm and salty Irminger Current (IC) to form the West Greenland Current (WGC). This latter follows the Greenland coast and then crosses Baffin Bay and joins water from the CAA and Nares Strait to form the Baffin Current (Melling et al., 2001), which flows southward to the Labrador Sea. The Arctic freshwater export to the North Atlantic Ocean is accomplished by three major gateways, which are Nares Strait, Fram Strait and the CAA via Lancaster and Jones Sounds (Dickson et al., 2007).

2.2. Last glacial conditions and oceanography in the CAA

The CAA is characterized by a large number of narrow channels between islands that were deepened by glacial and fluvial erosion during the Quaternary period. During the Last Glacial Maximum (LGM), most of the CAA was cover by the Innuitian ice-sheet (IIS), which was coalescent with the Greenland ice-sheet (GIS) along Nares Strait and with the Laurentide ice-sheet (LIS) along the 74°N of latitude. Due to this configuration, a zone of maximum ice thickness followed an NE-SW ridge (known as the Innuitian uplift) in the central CAA. Break-up of the IIS progressed from west to east beginning around 11,600 cal BP but Wellington channel was filled by an ice-stream until 8500 cal BP (Dyke et al., 2002; England et al., 2006). Similarly, the IIS and GIS remained in contact until 8500 cal BP feeding several ice-streams in northernmost Baffin Bay. (Dyke, 1998, 1999, 2008; Dyke et al., 2002; Zreda et al., 1999; England,

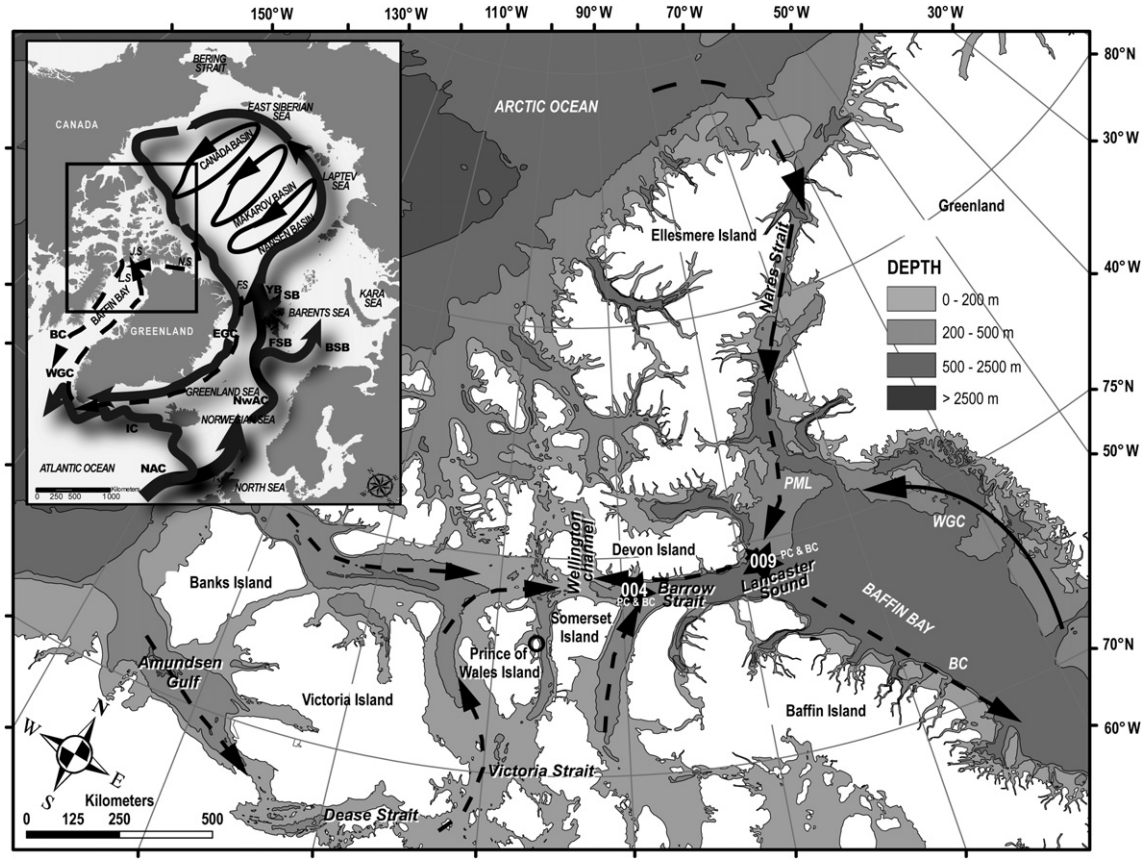

Fig. 1. (Inset) Map showing polar and Atlantic water masses exchange between the Arctic and North Atlantic Oceans. The North Atlantic water penetrating into the Arctic Ocean at depth ranging from 200 to 1700 m is schematically shown by black arrows, whereas dashed arrows correspond to the Arctic surface currents including freshwater export (NAC = North Atlantic Current; IC = Irminger Current; NwAC = Norwegian Atlantic water Current; BSB = Barents Sea branch; FSB = Fram Strait branch; YB = Yermak branch; SB = Svalbard branch; EGC = East Greenland Current; WGC = West Greenland Current; BC = Baffin Current). The EGC and WGC are a mixture of Atlantic water at mid-depth and Arctic surface water. The Arctic freshwater export is accomplished by Jones Sound (J.S), Lancaster Sound (L.S), Nares Strait (N.S) and Fram Strait (F.S). Location of the coring sites at the entrance of the Lancaster Sound and the Barrow Strait (black stars) with major surface currents in the CAA. The circulation in the CAA has an eastward component. Dashed black arrows correspond to the Polar Mixed Layer whereas the black arrow corresponds to the Atlantic water (BC = Baffin Current; WGC = West Greenland Current; PML = Polar Mixed Layer). The black circle between Prince of Wales and Somerset islands corresponds to Prescott Island. Modified from (Ledu et al., 2008).

1998, 1999; England et al., 2000, 2004, 2006; England and Lajeunesse, 2004; Atkinson and England, 2004).

As a consequence of this glacial history, about 70% of the CAA is shallower than 500 m (mean depth, 124 m) with a limiting sill at 125 m water depth located in Barrow Strait. Maximum depths are found at the entrance of Lancaster Sound (McLaughlin et al., 2004; Jakobsson, 2002, 2004; Prinsenberg and Bennett, 1987). The MANWP connects the eastern to the western Arctic through Lancaster Sound, Barrow, Victoria and Dease straits (Fig. 1). The NWP is generally recovered by heavy multi-year sea-ice at least in the central channels of the CAA. However, during the last two years, instrumentals data indicate that multi-year pack ice in these channels has decreased (Howell et al., 2009). First year sea-ice is present in the western and eastern part of the NWP with freeze up starting in November and minimum sea-ice extent in early September (Melling, 2002). The sea-surface temperature (SST) is about −1.8 °C during the period of sea-ice cover to −1.6 °C and +5 °C in late August–September, whereas the sea-surface salinity (SSS) is 32–33 in winter and ranges from 30 to 31 in the west to 32–33 in the east during summer (Prinsenberg and Hamilton, 2005; Mudie and Rochon, 2001).

The mean circulation has an eastward component (Fig. 1) because of steric sea-level effect between the North Pacific and the North Atlantic Oceans (Steele and Ermold, 2007; McLaughlin et al., 2004). The inflow of Atlantic water is strongly constrained by the shallow channels and only the entrance of Lancaster Sound received Atlantic water from the deflected WGC. (Prinsenberg and Hamilton, 2005). Elsewhere in the MANWP, the water column consists of a seasonal mixed layer lying on summer and winter Pacific water mass derived from the Canada Basin through M'Clure Strait and Amundsen Gulf (Jones et al., 2003).

Present day conditions in Lancaster Sound are 2 °C ± 1.2 °C for the summer (August) SSTs with summer (August) SSS of 31.3 ± 0.98. Sea-ice cover extends for 8.1 ± 0.9 months/year. In Barrow Strait, present summer (August) SSTs is 1.9 ± 1.7 °C with SSSs of 30 ± 1.24 and sea-ice cover of 10.2 ± 0.9 months/year (NODC, 2001; NSIDC, 1953–2000 data).

3. Material and methods

3.1. Sampling and palynological preparation

Sampling in Lancaster Sound and Barrow Strait (Fig. 1) was respectively carried out in the summer of 2004 and 2005 during legs 9 and 1 of the ArcticNet oceanographic campaigns on board the research ice breaker CCGS Amundsen. The sampling sites were selected using a Simrad EM 300 multibeam echo sounder and a Simrad 3.5 kHz sub-bottom profiler to avoid disturbed sediment areas (i.e., erosion, mudflows and/or mass movements). Cores 009 PC and BC (Lancaster Sound, 74°11.2′N/81°11.7′W, water depth

781 m, length 600 and 35 cm respectively) and cores 004 PC and BC (74°16.1′N/91°05.4′W and 74°16.1′N/91°04.4′W, water depth 350 m, length 670 and 35 cm respectively) were collected using a piston corer and a box corer. Each core was then sub-sampled every 10 cm (piston cores) and every 5 cm (box cores) for palynological analyses. Sub-samples were processed according to the standard palynological preparation described in Rochon et al., (1999). Five cm^3 of wet sediments were collected by distilled water displacement in a graduate cylinder. A tablet of marker grains (*Lycopodium clavatum* spores, University of Lund, 1984, Batch N°414831) of known concentration (12,100 ± 1892 spores per tablet) was added to each sample for calculating the concentration of palynomorphs. Sediments were then sieved using Nitex sieves of 100 and 10 μm mesh to eliminate coarse sand, fine silt and clay. The fraction between 100 and 10 μm was then stored in a tube with a few drops of phenol for subsequent chemical treatments.

The chemical processing consists of repeated hot HCl (10%, 4 treatments) alternating with hot HF (49%, 3 treatments) treatments to dissolve carbonate and silicate particles, respectively. The remaining fraction was then rinsed with distilled water to eliminate all traces of acid before a final sieving at 10 μm to remove the fluorosilicates and fine particles. Finally, this fraction was mounted in glycerine gel between slide and cover slide. Palynomorphs (dinocysts, pollen grains and spores, acritarchs, organic linings of benthic foraminifers, chlorococcales) were then systematically counted in transmitted light microscopy (Nikon Eclipse 80 − I) at 200–400×. A minimum of 300 dinocysts was counted in each sample in order to obtain the suitable statistical representation. Palynomorph concentrations were calculated using the marker grain method (Matthews, 1969) and expressed in terms of individuals per volume unit (palynomorph/cm^3).

3.2. Estimation of past sea-surface conditions

Dinoflagellates are planktonic unicellular organism living in the photic zone of the water column. About half of them are phototrophic (order Gonyaulacales), whereas others are heterotrophic (mainly belonging to the order Peridiniales), mixotrophic, parasitic or symbiotic. During sexual reproduction, some species form a highly resistant cyst composed of a complex biomacromolecular substance, called dinosporine (Kokinos et al., 1998; Versteegh and Blokker, 2004).

Many recent studies have shown a close relationship between dinocyst assemblages in surface sediments and sea-surface parameters (see Marret and Zonneveld, 2003 and de Vernal and Marret, 2007, for synthesis on the subject). In particular, it has been shown that annual thermal amplitude, salinity and duration of sea-ice cover are determinant factors on the distribution of dinocyst, notably in the North Atlantic (Rochon and de Vernal, 1994; Rochon et al., 1999; de Vernal et al., 1994, 1997, 2000), the Canadian Arctic including the Beaufort Sea, the Canadian Archipelago, the Northern Baffin Bay and Hudson Strait (Richerol et al., 2008a; Mudie and Rochon, 2001; Hamel et al., 2002), the Laptev Sea (Kunz-Pirrung, 2001), the Bering and Chukchi seas (Radi et al., 2001). The above mentioned studies have led to the development of a surface sediment reference database that is regularly updated (de Vernal et al., 1994, 2001; Rochon et al., 1999; Radi and de Vernal, 2008). The database used here contains 1189 reference sites of modern dinocyst spectra and corresponding values of sea-surface temperature (SST) and salinity (SSS) compiled from the 2001 version of the World Ocean Atlas (NODC, 2001). The seasonal duration of sea-ice cover is expressed as the number of months per year with more than 50% of sea-ice coverage after data from the National Snow and Ice Data Center (NSIDC, 1953–2000 data) in Boulder. Using the software R (http://www.r-project.org/), we applied the modern analogue technique (MAT) for the quantitative estimates of past sea-surface parameters because it required less data manipulation than other techniques with a root mean square error of prediction (RMSEP) among the lowest (Guiot and de Vernal, 2007; de Vernal et al., 2005a; de Vernal, 2009). Many studies have used MAT on Holocene Arctic marine cores, including Baffin Bay (Levac et al., 2001; Rochon et al., 2006), Chukchi Sea (de Vernal et al., 2005b; McKay et al., 2008), Beaufort Sea (Rochon et al., 2006; Richerol et al., 2008b), Laptev Sea (Kunz-Pirrung et al., 2001), Barents Sea (Voronina et al., 2001), Nares Strait (Mudie et al., 2006) and the eastern part of the CAA (Mudie et al., 2005; Ledu et al., 2008).

MAT as described by Guiot and Goeury (1996) and adapted by de Vernal et al. (2001; 2005a) yields good results as indicated by coefficients of correlation (R) greater than 0.93 between estimated and instrumentals hydrographic parameters and RMSEP that are close to the interannual variability recorded from instrumental measurements. The degree of accuracy of the estimated reconstructions (RMSEP) is obtained by the calculation of the standard deviation of the residual (estimated minus observed values), which is ±1.7 °C and 1.7 for SSTs and SSSs, respectively and ±1.1 month/year for the duration of sea-ice cover. However regarding SSSs, sites within the low salinity domain (<20) occurring in nearshore and shallow environments revealed large interannual variability. This is particularly critical for the CAA, where the reconstructed summer salinity data derived from MAT must be interpreted with caution.

3.3. Taxonomic considerations

The taxonomy of dinocysts used in this work conforms to that Rochon et al. (1999), de Vernal et al. (2001) and Head et al. (2001). Spiny round brown cysts occur frequently in high latitudes assemblages and represent a taxonomically diverse group. The cysts which were routinely identified include *Islandinium minutum* and *Islandinium cezare*. They differ principally on the basis of process terminations that are minutely expanded for the latter specie whereas the first specie is characterized by acuminate process type (Head et al., 2001). They also include *Echinidinium karaense* described by Head et al. (2001). Recently, Ledu et al. (2008) found some *Echinidinium* species in core from the easternmost part of the MANWP but difficulty in identifying at the species levels did not allow a clear distinction between species. In the present work, they are referred to as *Echinidinium* spp.. Similarly, some taxa were grouped because of similar morphological features and/or difficulties in seeing the archeopyle. This is the case for *Brigantedinium* spp., which include *Brigantedinium simplex* and *Brigantedinium cariacoense*, *Spiniferites elongatus* and *Spiniferites frigidus* are grouped together and *Operculodinium centrocarpum* includes all the morphotypes described in de Vernal et al. (2001) and Radi et al. (2001). Finally, the cyst of *Polykrikos* Arctic morphotype is distinguished by its smaller size and reduced ornamentation in comparison to the cyst of *Polykrikos schwartzii*. Illustrations of *Polykrikos* Arctic morphotype can be found in de Vernal et al. (2001), whereas details of the description can be found in Kunz-Pirrung (1998). The grouping of taxa for statistical purposes is conforming to that of the GEOTOP dinocyst nomenclature. List of dinocyst taxa and those resulting from grouping are available on the GEOTOP web site (http://www.geotop.ca).

3.4. Geochemical and isotopic content, grain size and magnetic susceptibility

Organic carbon (C_{org}), nitrogen (N) and inorganic carbon (C_{inorg}) contents were measured using a Carlo-Erba elemental analyser NC 2500 at the Geochemistry and Geodynamics Research Center

(GEOTOP). The procedure consists of taking a sediment sample aliquot that is dried, ground and analysed for its total carbon and nitrogen content. A second aliquot is acidified with HCl (1 N) in order to dissolve carbonates, washed and analysed for C_{org} content. C_{inorg} is then calculated by the difference between the two measurements. The $CaCO_3$ content of each sample was determined from the molar weight of $CaCO_3$ (100 g) and its content in C_{inorg} (12 g) allowing to calculating the calcium carbonate equivalent. Very little biogenic carbonates were observed in the sediments. Therefore, the major part of the $CaCO_3$ content in sediments of the study area is most likely due to detrital continental inputs. The carbon isotopic composition of organic matter ($\delta^{13}C$) was measured on the acidified aliquot by continuous-flow mass spectrometry using a Carlo-Erba elemental analyser connected to an Isoprime mass spectrometer.

Grain size analysis (0.04–2000 μm) was performed at the Institut des sciences de la mer de Rimouski (ISMER) using a Beckman-Coulter LS 13320 laser diffraction grain size analyser. The software Gradistat (Blott and Pye, 2001) was used to derive the grain size distribution and statistical parameters (mean and standard deviation). The whole core volumetric magnetic susceptibility was determined at 1 cm intervals for core 009 PC and 2 cm intervals for core 004 PC, using a GEOTEK Multi Sensor Core Logger (MSCL) on board the CCGS Amundsen.

3.5. Paleomagnetic measurements

Paleomagnetic measurements for cores 009 and 004 PC were carried at the Sedimentary Paleomagnetism Laboratory at ISMER, using a 2-G Enterprises Model SRM-755 cryogenic magnetometer. The natural remanent magnetization (NRM) was measured on u-channels (rigid u-shaped plastic liners with a square 2 cm cross section and a length of 1.5 m) at 1 cm intervals. However, due to the finite spatial resolution of the magnetometer's pickup coils, each measurement integrates a stratigraphic interval of 7 cm. In order to eliminate this edge effect, the data from the upper and lower 7 cm of each u-channel were excluded. To isolate the characteristic remanent magnetization (ChRM), the NRM was measured and progressively demagnetized applying peak alternative fields (AF) of 0–80 mT at 5 mT increments. The component inclination of the ChRM (ChRM I) was calculated at 1 cm intervals using a least-square line fitting procedure (Kirschvink, 1980). Using the software developed by Mazaud (2005), we also calculated the maximum angular deviation (MAD) to estimate the quality of the directional data.

3.6. Color reflectance

Diffuse spectral reflectance was measured with an X-Rite digital swatch book DTP-22 hand-held spectrophotometer. Reflectance data were then converted in the L* a*b* color space. High values (low values) of L* indicate white (black) color, whereas positive (negative) values of a* indicate red (green) and positive (negative) values of b* correspond to yellow (blue). The L* a* b* data were used to estimate missing sediment due to the piston coring process (Fig. 2).

3.7. Initial chronology of the cores

A constant rate supply ^{210}Pb model (Appleby and Oldfield, 1983) was used to estimate ages and to determine sedimentation rates in cores 009 BC and 004 BC (Fig. 3A). Data for core 009 BC indicate negligible biological mixing at the top of the sequence and the ^{210}Pb in excess in the upper 15 cm of the core suggests an average sedimentation rate of about 60 cm/kyr. Assuming a constant sediment accumulation rate from the top to the base of the core, the sequence would cover approximately the last 580 years, from about AD 1420 at the base to the beginning of AD 2000 at the top. In contrast, biological mixing was observed in the uppermost part of the core 004 BC down to ~1.5 cm. The data from this zone were not used for establishing the chronology using the ^{210}Pb in excess. Apart from the bioturbation mixing zone, the ^{210}Pb in excess in the upper 20 cm indicates sedimentation rates ranging from 212 cm/kyr at the base to the middle part of the core to 33 cm/kyr in the upper part of the core. Using these sediment accumulation rates, and assuming sedimentation rate ranging from 20 cm to 35 cm, we calculated that core 004 BC spans the last 400 years, from about AD 1600 at the base to AD 2000 at the top.

An initial chronostratigraphy for cores 009 and 004 PC was established using calibrated AMS-^{14}C dates on mollusk shells and mixed benthic foraminifers (Ledu et al., 2007, 2008). All radiocarbon ages were calculated using Libby's half-life (5568 years) and corrected for natural and sputtering fractionation ($\delta^{13}C = -25‰$ VS-PDB). The online Calib V 5.0.2 software was used to convert conventional ^{14}C ages into calendar years using the marine04 calibration curve (Hughen et al., 2004). In addition to the usual air–sea $^{14}CO_2$ reservoir difference (400 years), a regional correction (ΔR) of 400 years (i.e., total correction of 800 years) has been applied (Mangerud and Gulliksen, 1975; Blake, 1987; Table 1). An initial age-depth model based on linear interpolation was constructed for each core assuming constant sedimentation rate between the calibrated age data points. For core 004 PC, this was done using a composite depth scale corrected for missing sediments due to the piston coring process. The comparison of the magnetic susceptibility and the reflectance (L*) data in the piston and trigger weight cores (004 PC and 004 TWC, respectively), reveals that about 50 cm of surface sediment was lost during piston coring (Fig. 2). Note that all depths of core 004 PC are expressed in corrected depth, which account for the missing sediment. In contrast, no estimation of missing sediment has been made for core 009 PC due to the poor recovery of the trigger weight core. The age-depth models indicate that core 009 PC spans about 11,000–2000 cal BP, whereas core 004 PC spans the last 11,400 cal BP, which represents most of the Holocene. The calculated sedimentation rates ranged from 45 to 122 cm/kyr and from 27 to 141 cm/kyr for core 009 and 004 PC, respectively (Background Data Set, Fig. 3B).

4. Results

4.1. Construction of a composite age-depth model based on paleomagnetic secular variation and harmonic spherical model of the geomagnetic field correlation

Various studies have documented significant directional changes (inclination and declination) of the Earth's magnetic field during the Holocene in high latitudes (Baffin Bay, central Finland, northern Sweden, St Lawrence estuary, Siberia, Russia, Fennoscandia, Iceland, Beaufort and Chukchi seas, Canadian Arctic and Alaskan margins; e.g., Andrews and Jennings, 1990; Saarinen, 1998; Snowball and Sandgren, 2002; St-Onge et al., 2003; Korte et al., 2005; Korte and Constable, 2005; Snowball et al., 2007; Stoner et al., 2007; Barletta et al., 2008a; Besonen et al., 2008; Lisé-Pronovost et al., 2009). These geomagnetic directional changes also known as paleomagnetic secular variation (PSV) have been used as a dating method (e.g., Saarinen, 1999; Kotilainen et al., 2000; Breckenridge et al., 2004; St-Onge et al., 2003, 2004; Stoner et al., 2007; Barletta et al., 2008b; Lisé-Pronovost et al., 2009). In Arctic sediments where biological remains, such as foraminifers or mollusk shells are generally poorly preserved

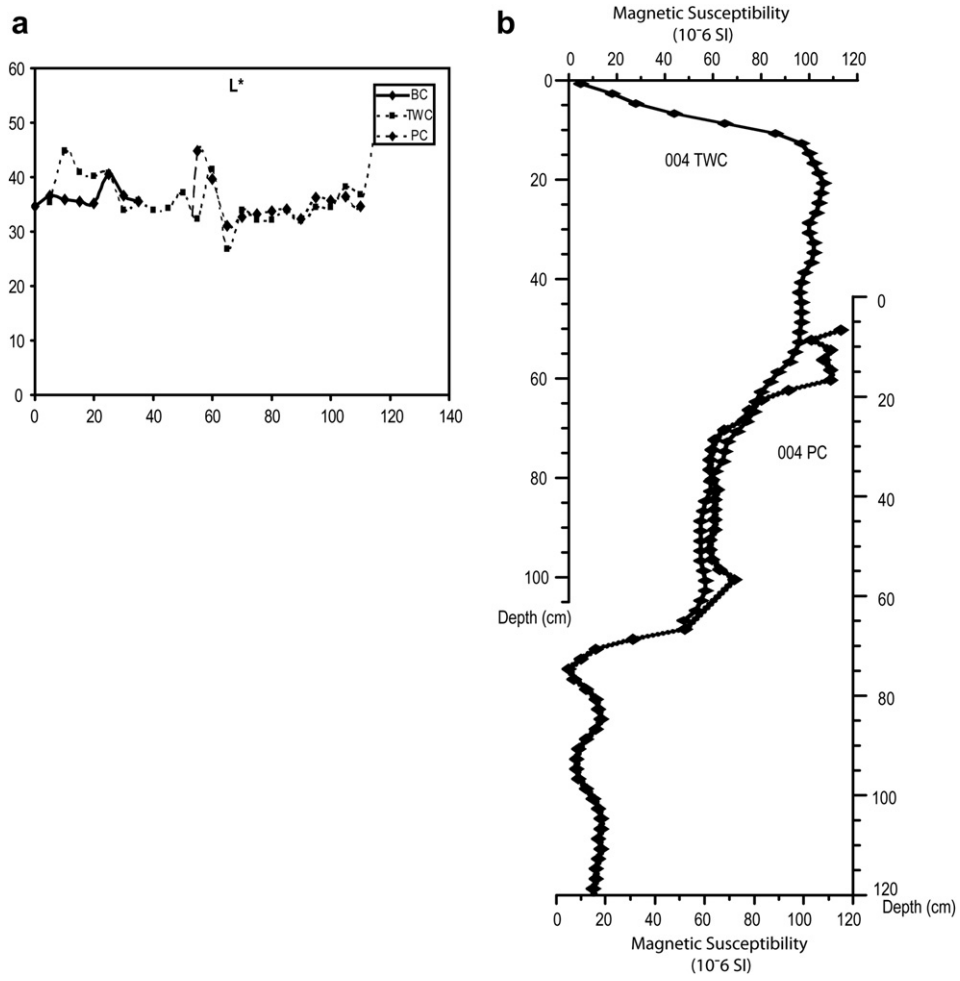

Fig. 2. (a) Diagrams showing the color reflectance (L*) for cores 004 PC, TWC and BC, used here to estimate top piston core sediment missing due to piston coring process. (see text for details). (b) Diagram showing the magnetic susceptibility for cores 004 PC and TWC. Diagrams (a) and (b) suggest that about 50 cm of sediment from core 004 PC was lost during coring process.

because of calcium carbonate dissolution, PSV correlation can be useful to improve the chronostratigraphical framework. The paleomagnetic data of core 009 PC shows a strong and stable well-defined component magnetization as indicated by low MAD values (MAD $\leq 2^{\circ}$). In contrast, core 004 PC depicts MAD values above 10° between 460 and 410 cm and between 410 and 150 cm. Such values indicate directional data of low quality (e.g., Stoner and St-Onge, 2007). However, between 50 cm and 150 cm, MAD values are less than 10°, suggesting that the directional paleomagnetic data in the upper part of the core is of better quality (Fig. 4). Nonetheless, between the top of the core and 60 cm, inclination values are relatively shallow compared to the expected values based on a geomagnetic axial dipole model (GAD = 80°) and were thus excluded. Using the predicted inclinaison data for our coring sites over the last 7000 years derived from the spherical harmonic model of the geomagnetic field, CALS7 K.2 model (Korte et al., 2005; Korte and Constable, 2005), we correlated the inclination record of the upper part of core 004 PC with the predicted inclinaison calculated using the CALS7 K.2 model. Similarly, we correlated the inclination record of core 009 PC with the predicted inclination record derived from the CALS7 K.2 model (Fig. 4, Table 2). Recently, Barletta et al. (2008a) and Lisé-Pronovost et al. (2009) showed a strong consistency between the calculated inclination using the CALS7 K.2 spherical harmonic model and inclination records in cores from the Chukchi and Beaufort seas and the Alaskan margin. Due to their proximity to the North Magnetic Pole, cores from the high latitudes have the potential to record higher amplitude directional changes, which are well represented by the CALS7 K.2 model at the millennial to centennial time scale (Barletta et al., 2008a).

This exercise results in five and seven inferred additional ages for cores 009 PC and 004 PC, respectively. A new age-depth model for each core was then constructed using the CALS7 K.2 correlation. A second-order polynomial fit was used to derive an age-depth model for core 009 PC, whereas an interpolation fit was used for core 004 PC (Fig. 5). One measured calibrated AMS-^{14}C date in core 004 PC (Beta − 213845) has been excluded from the age-depth model because it appears clearly to be an outlier when compared with the other radiocarbon dates on the PSV correlation probably due to reworking of the mollusk shell fragments in the core. As a result, 9 dates were used for the age-depth model of core 009 PC (5 dates derived from the CALS7 K.2 inclination correlation and 4 calibrated AMS-^{14}C dates) and 10 dates for core 004 PC (7 dates from the CALS7 K.2 correlation and 3 calibrated AMS-^{14}C dates). In order to test the accuracy of our age-depth models, we compare the magnetic inclination of cores 009 PC and 004 PC based on their new chronology (Fig. 6) with the inclination profiles of Holocene sediment cores from the Arctic (Beaufort and Chukchi seas; Barletta et al., 2008a). Major shifts in the magnetic inclination are recorded around 1000, 1500, 2500, 3500, 4500, 5500 cal BP and are on

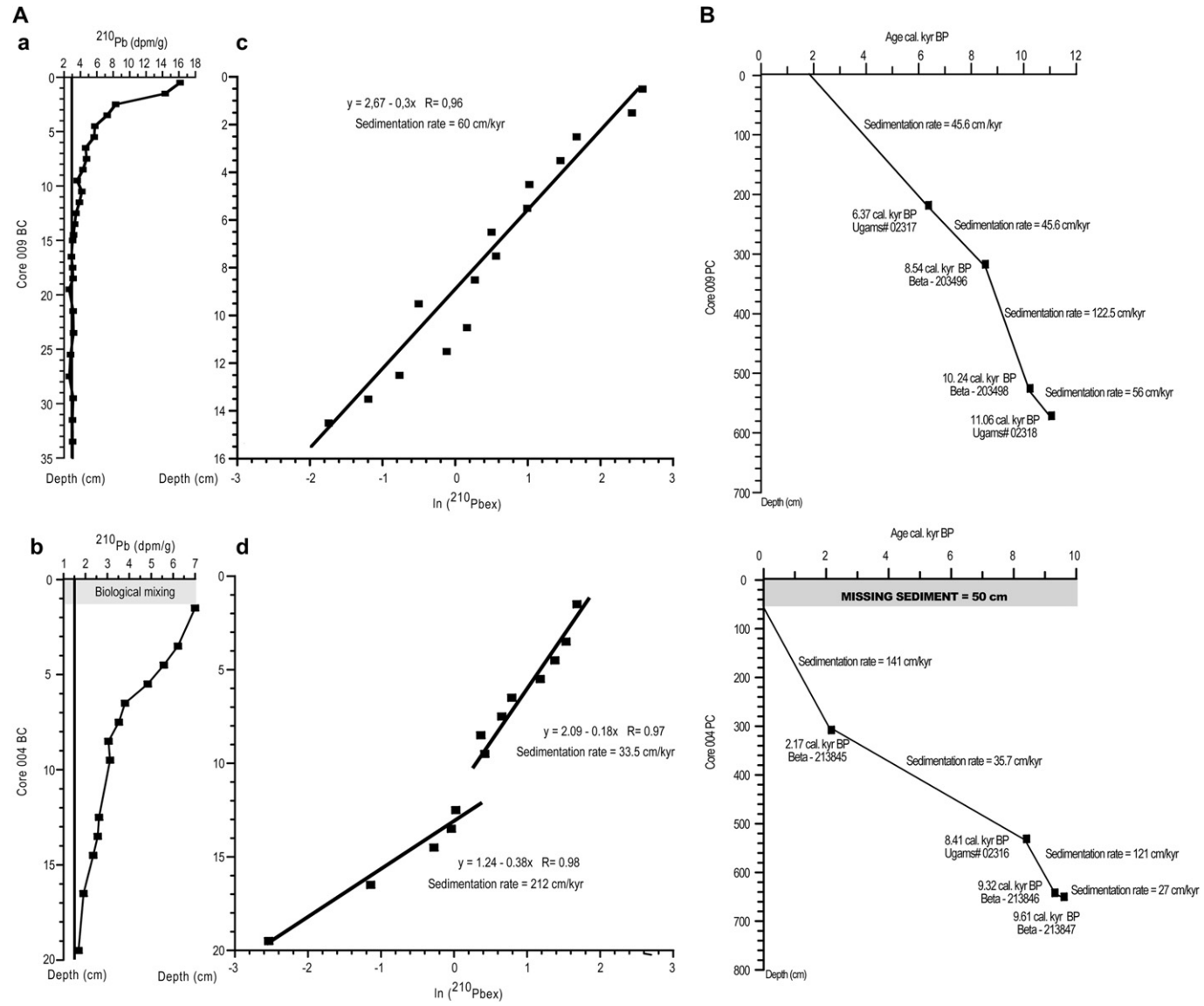

Fig. 3. A (A and B) Diagrams showing the ^{210}Pb activity in core 009 and 004 BC. The vertical grey lines (asymptote = 3 for core 009 BC and 1.5 for core 004 BC) correspond to supported ^{210}Pb. (c and d) Diagrams showing the Neperian logarithm of the excess ^{210}Pb, which is used for estimating sedimentation rates. Sedimentation rates are 60 cm/kyr in core 009 BC and ranges from 33.5 to 212 cm/kyr in core 004 BC. B. (Background Data Set). Initial age-depth models for cores 009 and 004 PC, respectively. Both age models are based on linear interpolation fit between calibrated AMS-^{14}C and indicate sedimentation rates ranging from 45 to 122 cm/kyr and from 27 to 141 cm/kyr for cores 009 and 004 PC, respectively. The grey zone corresponds to the missing sediment due to piston coring process.

average 225 ± 55 yr from those observed in core 009 and 004 PC. These shifts were consistent with the inclination predicted by the CALS7 K.2 model but also with the major shifts recorded in lake cores from North America (Verosub et al., 1986; Geiss and Banerjee, 2003) and in cores from the Arctic Ocean (Barletta et al., 2008a; Lisé-Pronovost et al., 2009). Even in core 004 PC, where the directional data is more unstable, these shifts are relatively well marked. However, to support our new age-depth model for this core, we also compare the linear interpolation fit used to construct the age-depth relationship with the isostatic emergence curve near Barrow Strait area (Dyke, 1998). The curve indicates that the maximum emergence rate took place between 8500 and 5000 cal BP with ~100 m of emergence, which ~80 m have been accomplished in 1500 years (between 8500 and 7000 cal BP). This is also the time interval where the linear interpolation fit for core 004 PC age-depth model indicates maximum sedimentation rates (Fig. 5).

The age-depth models indicate that core 009 PC covers the last 11,100–2000 cal BP and core 004 PC covers the last 10,800–900 cal BP (Fig. 5). The calculated sedimentation rates range from 43 to 140 cm/kyr and from 15 to 118 cm/kyr for core 009 PC and 004 PC, respectively, allowing for a centennial to millennial time scale resolution.

4.2. Lithology, grain size and magnetic susceptibility

Sediments from 600 to 560 cm in core 009 PC consist of brown sand silty clay (2.5Y 5/2, Munsell color chart). From 560 cm to the top of the core, the sediment consists of olive green silty clay (5Y 4/3) with mottles ranging from 3 to10 μm between 250 and 280 cm. Olive green silty clay (5Y 4/3) is also observed throughout core 009 BC. From 720 to 530 cm, core 004 PC consists of olive brown mud (2.5Y 4/3), whereas from 530 cm to the core top sediment consists in alternating olive grey mud (5GY 4/1) and dark olive brown-black mud (5Y 2/2). Finally, the sediment of core 004 BC consists of olive brown mud (2.5Y 4/3).

Table 1
Radiocarbon ages used to develop initial age-depth models for cores 2004-804-009 PC and 2005-804-004 PC.

Cores ID	Depth (cm)	Material dated	Laboratory numbers	Conventional radiocarbon ages (yr BP)[a]	Calibrated ages (cal. kyr BP)[b]
2004-804-009 PC	217–220	Mixed benthic foraminifers	Ugams# – 02317	6370 ± 30	6.37
2004-804-009 PC	317	Bivalve shell fragments	Beta – 203496	8490 ± 40	8.54
2004-804-009 PC	525	Bivalve shell fragments	Beta – 203498	9770 ± 50	10.24
2004-804-009 PC	571–572	Mixed benthic foraminifers	Ugams# – 02318	10,480 ± 40	11.06
2005-804-004 PC	258 (308*)	Bivalve shell fragments	Beta – 213845	2900 ± 40	2.17
2005-804-004 PC	481 (531*)	Benthic foraminifers	Ugams# – 02316	8350 ± 30	8.41
2005-804-004 PC	592 (642*)	Bivalve shell fragments	Beta – 213846	9060 ± 50	9.32
2005-804-004 PC	600 (650*)	Bivalve shell fragments	Beta – 213847	9320 ± 60	9.61

*Numbers in brackets are the corrected depth due to lost of sediment during piston coring process.
[a] This column lists the AMS-^{14}C ages as reported from the laboratory after normalisation for a δ^{13}C value of −25‰.
[b] Calibrated ages were estimated using the software CALIB 5.0.2 (Stuiver et al., 2005) with Delta R (ΔR) local reservoir effect of 400 years, which means a total correction of 800 years to account for the air–sea reservoir difference. The calibrated ages are computed from the arithmetic average of the calibrated age range, based on two standard deviations (i.e., a confidence interval of 95%).

Grain size analysis shows that silt and clay are predominant in most part of core 009 PC, representing ~60 and 40% of the grain size fraction, respectively (Fig. 7). Only the lower part of the core records higher percentages of sand (25–50%) and coarse silt. Core 004 PC is characterized by an absence of sand and the predominance of silt, representing more than 75% of the grain size fraction (Fig. 8). In core 009 BC silt and clay comprise about ~75 and 25% of the sediment respectively. Similarly, sediment in core 004 BC is characterized by high percentages of silt (85%).

Geochemical analyses of core 009 PC indicates that total carbon range from 6% to 3%, with higher values between 11,100 and 10,800 cal BP (Fig. 7). Organic carbon values ranges from 0.35 to 2% with values increasing gradually from the base to the top of the core, whereas inorganic carbon records values of 6% at the base of the sequence (11,100 to 10,800 cal BP) to 1% at the top. The isotopic composition of organic carbon (δ^{13}C) ranges from −26‰ VS-PDB at the base of the core (11,100 to 10,800 cal BP) to −22.5‰ VS-PDB at the top of the core. The C/N ratio shows values ranging from 30 at the base of the core

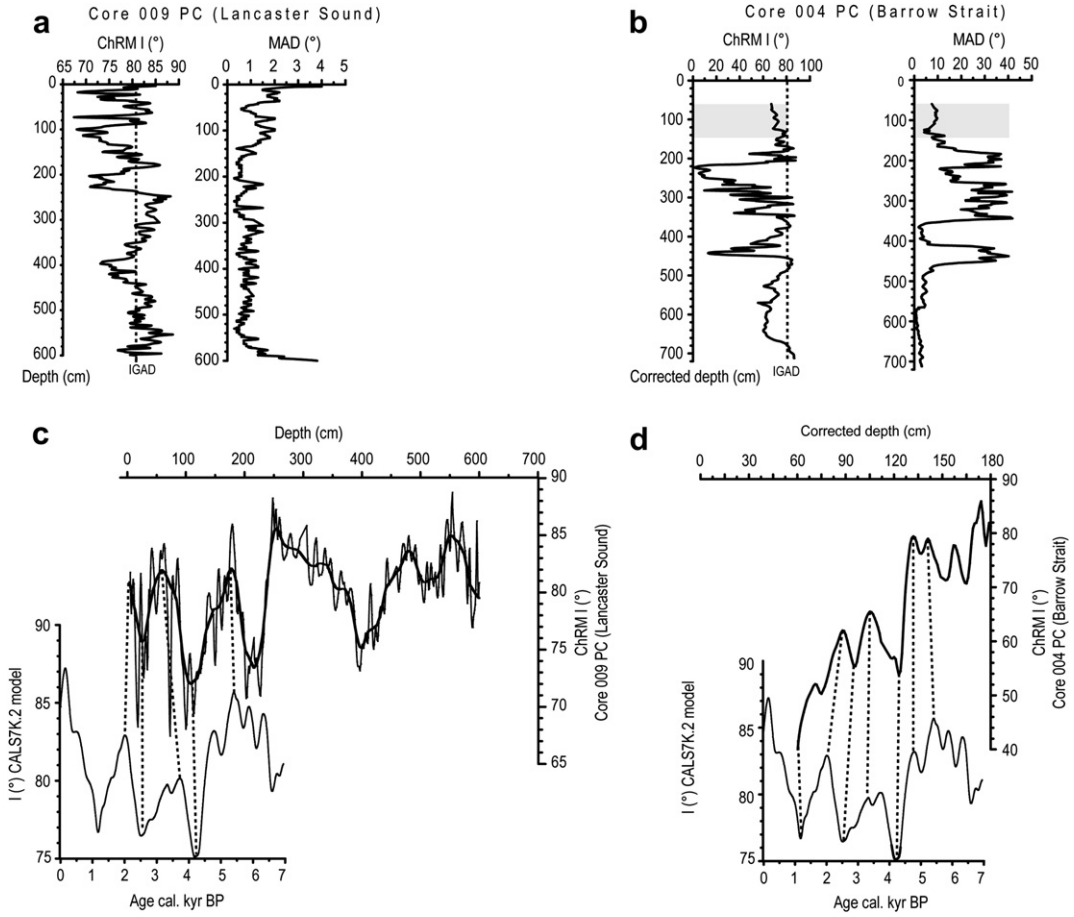

Fig. 4. (a and b) Diagrams showing the characteristic remanent magnetization of the component inclination (ChRM I) and the maximum angular deviation (MAD) values for core 009 and 004 PC. The vertical dashed line is the value of the geocentric axial dipole (GAD) for the ChRM I at both sites. The grey zones correspond to the zone used for correlation of paleosecular variation of the ChRM I (see text for details). (c and d) ChRM I for core 009 PC and ChRM I for the upper part of core 004 PC and the suggested correlation (dashed lines) with the CALS7 K.2 spherical harmonic model (Korte et al., 2005; Korte and Constable, 2005) of the predicted I (○) for both sites. Note that the first correlation in the uppermost part of core 009 PC is only suggested and was not used to construct the age-depth model.

Table 2
Measured calibrated radiocarbon ages and PSV correlation used to construct new age-depth models.

Cores	Measured calibrated years (cal. kyr BP)	Depth (cm)	CALS7 K.2 ages (cal. kyr BP)	Depth equivalence (PSV correlation cm)
2004-804-009 PC	6.37	217–220 (218.5[a])		
	8.54	317	2.5	25
	10.24	525	3.8	60
	11.60	571	4.2	105
			5.4	175
2005-804-004 PC	8.41	531*	1.2	60*
	9.32	642*	2	87*
	9.61	650*	2.5	96
			3.25	105*
			4.2	123*
			4.8	132
			5.4	141

*Corrected depth for missing sediment due to piston coring processes (see Fig. 3 and text for details).
[a] (*mean depth).

(11,100–10,800 cal BP) to 10 at the top. Finally, detrital CaCO3 records higher values at the base of core (~46%), which gradually decreases (~10%) at the top of the core, as does magnetic susceptibility.

Core 004 PC records values of total carbon around 5.5% in the most part of the core (Fig. 8). Organic carbon values displays values from 1% to 2.3% with increasing values from the base to the top of the sequence. Inorganic carbon records values of 3% in most of the sequence and $\delta^{13}C$ depicts its lowest values at the base of the core (from $-26‰$ to $-25.5‰$ VS-PDB during the interval 10,800–8500 cal BP). In contrast, the C/N ratio is relatively high at the base of the core (10,800 and 8500 cal BP) with values around 30, and gradually decreases towards the top of the core reaching 10. Similarly magnetic susceptibility records relatively high values from 10,800 to 8500 cal BP. Finally detrital $CaCO_3$ shows values around 30% in the most part of the sequence.

Geochemical analyses in core 009 BC indicate relatively constant values along the core with total carbon of 3%, C_{org} content of 2%, C_{inorg} values of 0.5% and $\delta^{13}C$ values of $-22.5‰$ (Fig. 7). The C/N ratio is about 11, whereas the $CaCO_3$ records values of 5%. Core 004 BC records also relatively constant values with total carbon of 5.5%, C_{org} content around 2% and C_{inorg} values of 3.5%, whereas C/N ratio is about 10 and $CaCO_3$ around 30% (Fig. 8).

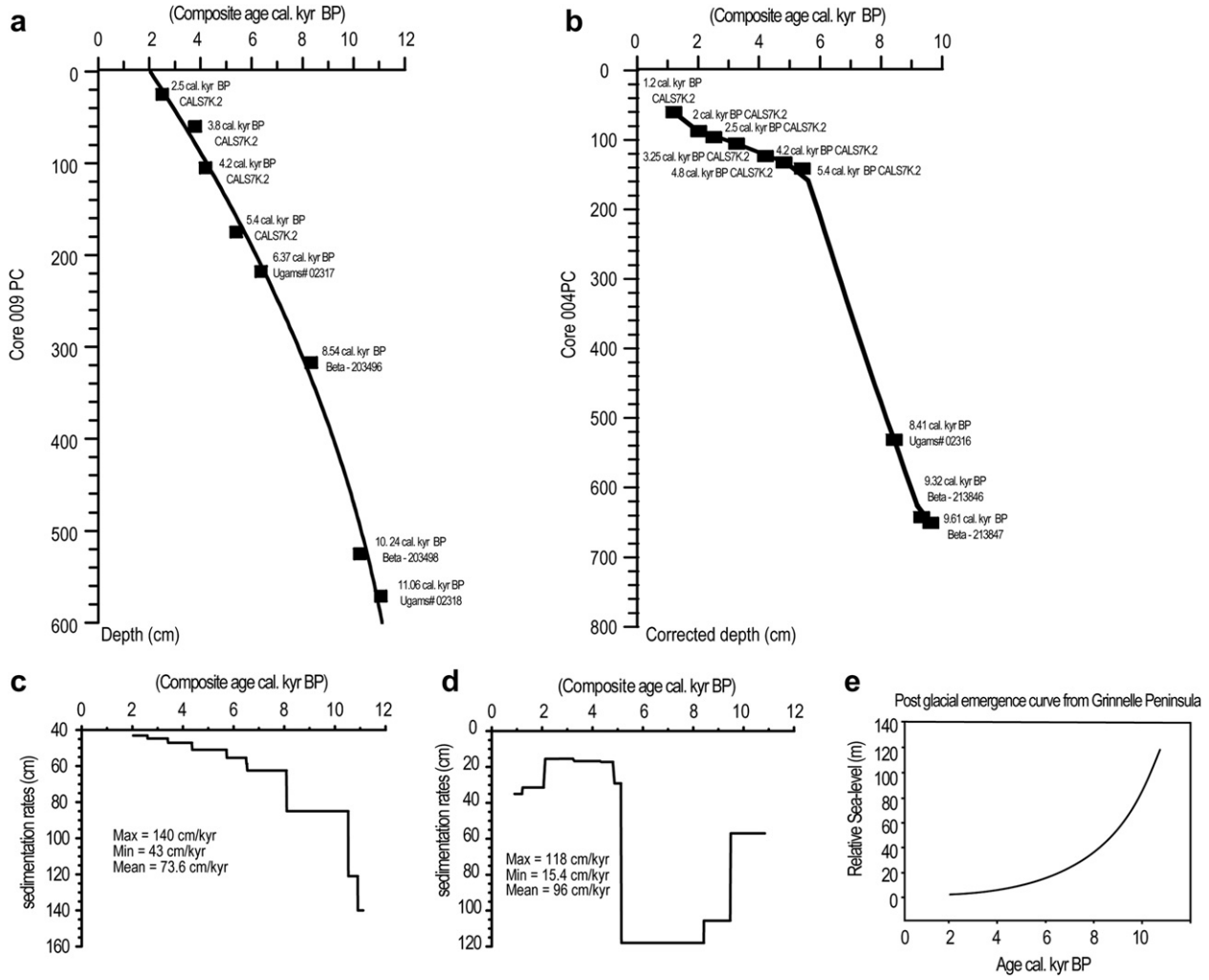

Fig. 5. (a and b) Composite age-depth model for cores 009 and 004 PC based on correlations between paleomagnetic secular variations of the geomagnetic field (ChRM I) and the CALS7 K.2 predicted inclination for both sites with initial AMS-^{14}C ages (see text and Table 2 for details). The age-depth model is based on a 2nd-order polynomial fit for core 009 PC and a linear interpolation fit for core 004 PC. (c and d) Sedimentation rates as suggested by the age-depth models. (e) Post-glacial emergence curve from Grinnelle Peninsula (northeast Barrow Strait), showing a maximum emergence rate between 8.5 and 5000 cal BP, consistent with the high sedimentation rates suggested by the age-depth model of core 004 PC during that interval. Modified from Dyke (1998).

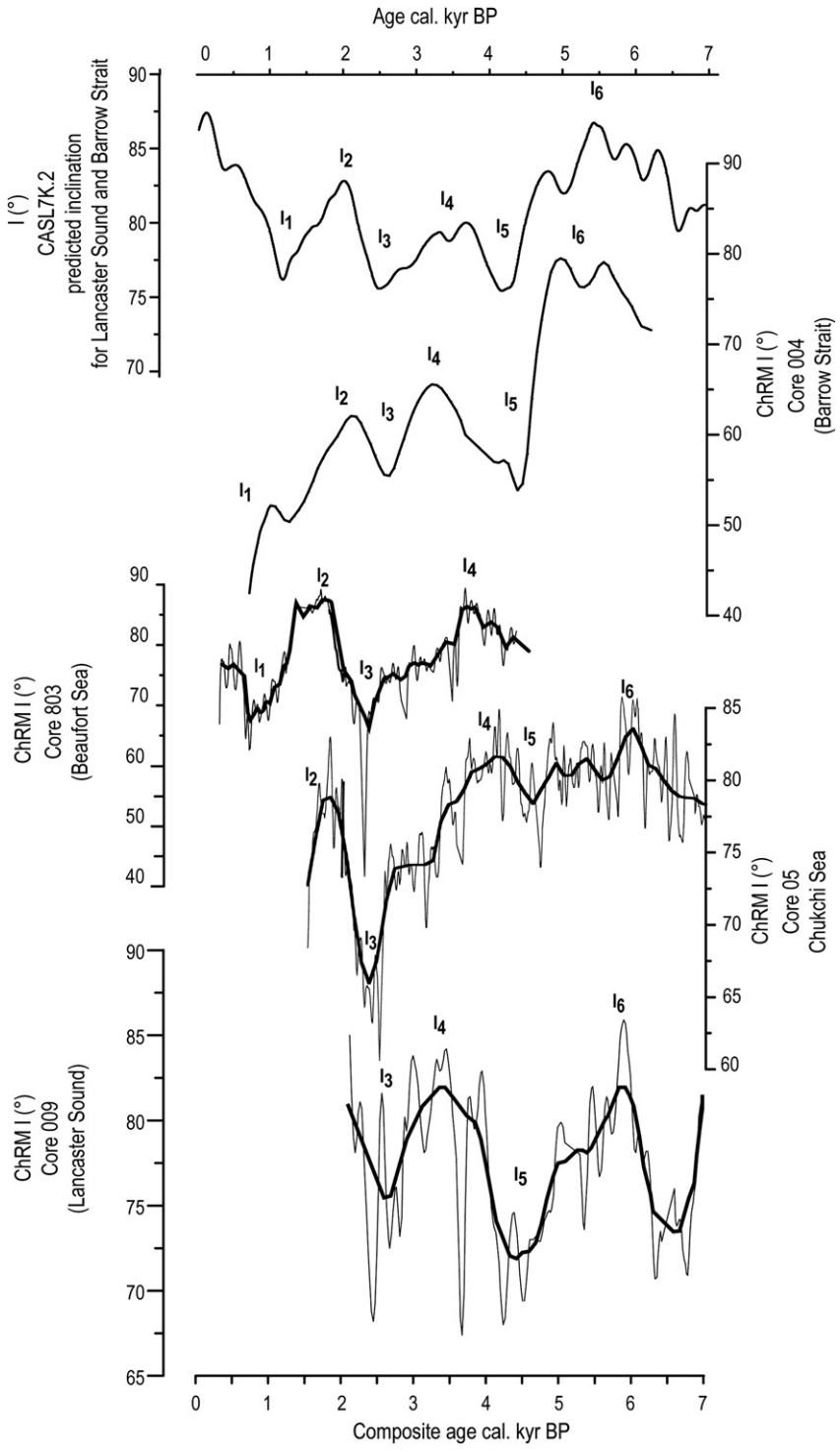

Fig. 6. Comparison of the characteristic remanent magnetization of the component inclination (ChRM I) between cores 009, 004 PC and other cores from the Chukchi and Beaufort seas (Barletta et al., 2008a). The thicker black lines represent weighted functions. Cores 009 and 004 PC are on their new composite chronology (see text for details). The uppermost diagram corresponds to the CALS7 K.2 spherical harmonic model of the predicted I (○) for Lancaster Sound and Barrow Strait (Korte et al., 2005; Korte and Constable, 2005). Major ChRM I shifts are observed in all records and occurred around 1000 (I_1), 1500 (I_2), 2500 (I_3), 3500 (I_4), 4500 (I_5), 5500 (I_6) cal BP.

4.3. Dinocyst assemblages and quantitative estimates of past sea-surface parameters

Cores 009 and 004 PC show well-preserved dinocyst throughout the sequence (Figs. 9 and 10), except in the lowermost part of core 009 PC, between 11,100 and 10,800 cal BP, where they are absent. Dinocyst assemblages reveal low species diversity, which is consistent with previous work in the CAA (Mudie and Rochon, 2001). Indeed, core 009 PC is dominated by four taxa that make up 90% of the assemblage: *Brigantedinium* spp., *I. minutum*, *Spiniferites elongatus/frigidus* and *O. centrocarpum*. In core 004 PC, 90% of the assemblages are dominated by two taxa: *Brigantedinium* spp. and *Islandinium minutum*.

The ratio of phototrophic to heterotrophic dinocyst taxa (G/P ratio) records low values in the most part of core 009 PC, indicating

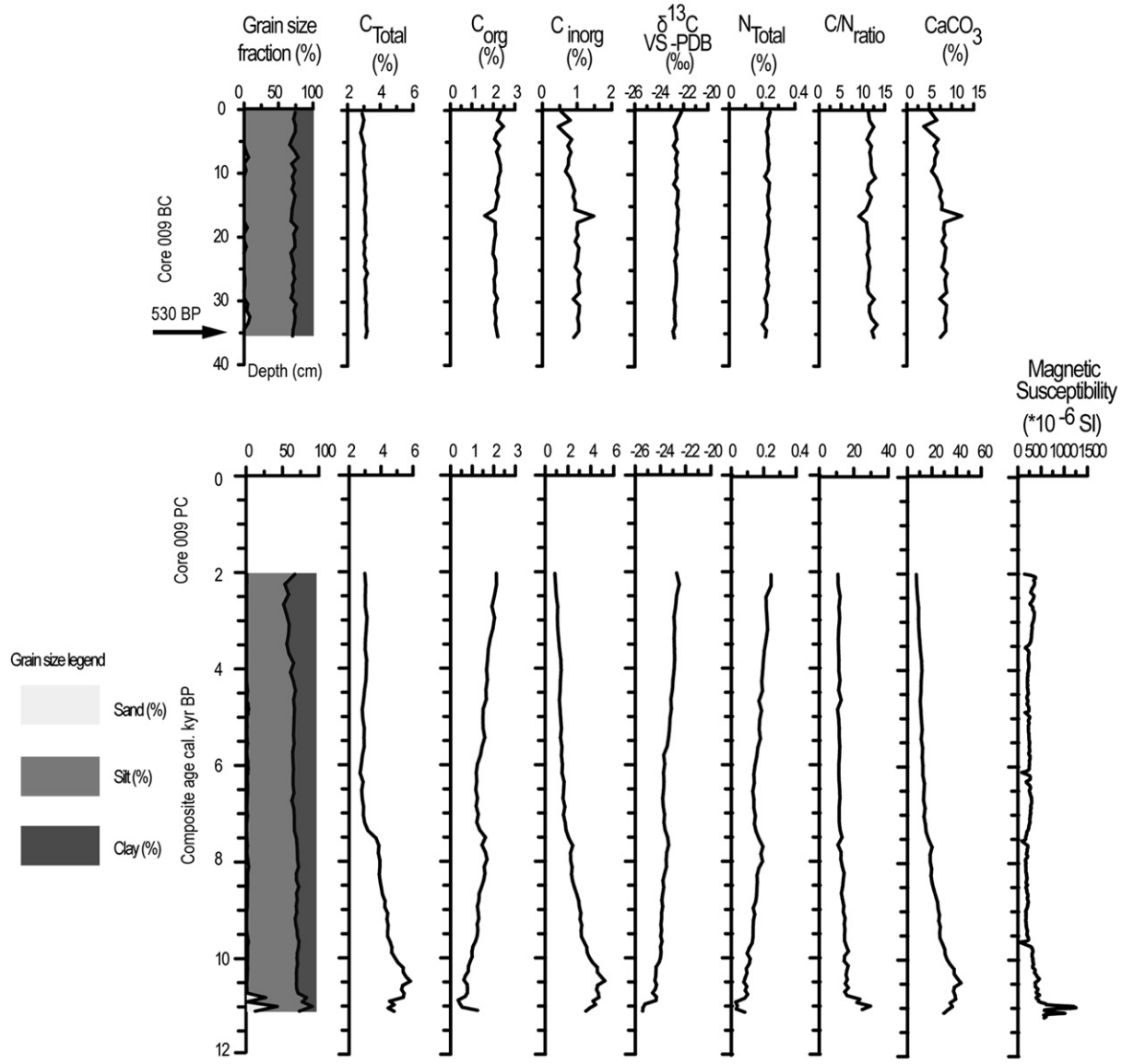

Fig. 7. Sedimentological (grain size), geochemical content of cores 009 PC and 009 BC. The chronology of core 009 BC is estimated from ^{210}Pb measurements and was converted from AD to cal BP ages. (Modified from Ledu et al., 2008).

the dominance of non-phototrophic taxa, except between 8500 and 4000 cal BP, where it reaches values ≥ 1. In contrast, photosynthetic taxa are absent throughout the length of core 004 PC. Dinocyst concentrations range from 1766 to 15230 cysts/cm^3 (average 6378 cysts/cm^3) and from 1634 to 12407 cysts/cm^3 (average 4739 cysts/cm^3), in core 009 and 004 PC, respectively.

Based on the relative abundance of dinocyst taxa, core 009 PC shows four different zones (Fig. 9). The first zone (from 11,100 to 10,800 cal BP) is characterized by the absence of dinocysts. The second zone (from 10,800 to 9000 cal BP) is dominated by the heterotrophic taxa, *Brigantedinium* spp. and *I. minutum*, representing 75 and 20% of the assemblages, respectively. Quantitative estimates of past sea-surface conditions suggest low SSTs (August) of 0 °C on average, which is about 2 °C colder than modern values, accompanied with sea-ice cover of 10 months/year, which is about 1 month/year more that at present. The third zone (from 9000 to 4000 cal BP) is marked by an increase in the relative abundance of the phototrophic taxa *O. centrocarpum* (50%), *Spiniferites elongatus/frigidus* (20%) and *Pentapharsodinium dalei* (5%). Sea-surface reconstructions suggest SSTs (August) reaching about 4.5 °C, which is 3 °C warmer than modern conditions, but with SSSs of about 25, which is lower than at present. Finally, the fourth zone (after 4000 cal BP) is again dominated by *Brigantedinium* spp. and *I. minutum* marking the establishment of modern conditions.

Based on dinocyst assemblages, core 004 PC shows three different zones (Fig. 10). The first zone (from 10,800 to 8500 cal BP) is dominated by the heterotrophic taxa *Brigantedinium* spp. (70%) and *I. minutum* (25%). The reconstructed sea-surface parameters indicate relatively low SSTs (August, on average 1 °C) and sea-ice cover of about 9 months/year, which is about 1.5 month/year less than modern conditions. The second zone (from 8500 to 5500 cal BP) is also marked by the dominance of *Brigantedinium* spp. and *I. minutum* but with an increase of dinocyst diversity as shown by the presence of *Islandinium*? *cezare* (10%), *Echinidinium aculeatum* (5%), *Echinidinium karaense* (3%) and the cyst of *Polykrikos* Arctic morphotype (10%), reaching their maximum relative abundance around 8500 cal BP. Quantitative estimates of past sea-surface conditions suggest warmer (~3 °C) SSTs (August) than modern around 8500 cal BP, decreasing SSSs (minimum around 15) and sea-ice cover (1.5 month/year lower than modern conditions). After this

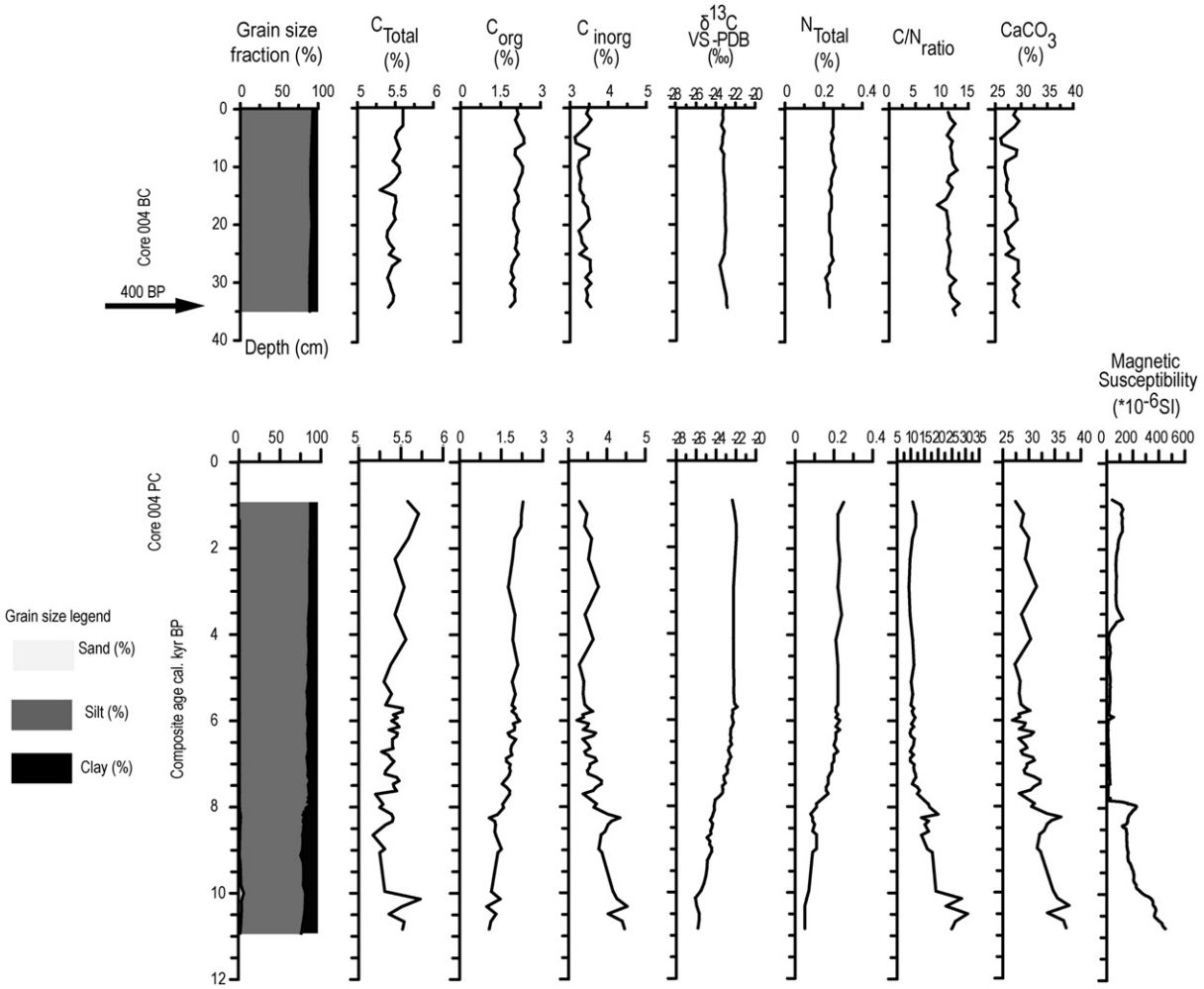

Fig. 8. Sedimentological (grain size), geochemical content of cores 004 PC and 004 BC. The chronology of core 004 BC is estimated from ^{210}Pb measurements and was converted from AD to cal BP ages.

interval, relatively harsh conditions prevailed, with lower SSTs (August, 0 °C on average) and variation of sea-ice cover (minimum of 9 and maximum of 11 months/year). Finally, the third zone (after ~5500 cal BP) is also characterized by an increase of dinocyst species diversity but more pronounced than in zone II reflecting a general trend towards warmer conditions as suggested both by the reconstructed SSTs (August, 3 °C warmer than modern) and the reconstructed sea-ice cover (2 months/year lower than modern conditions).

Core 009 BC also shows well-preserved dinocyst assemblages (Fig. 9) with concentrations ranging from 2220 to 4532 cysts/cm^3 (average 3623 cysts/cm^3). The G/P ratio records low values (<1), indicating the dominance of heterotrophic taxa, mainly *Brigantedinium* spp. (40%) and *I. minutum* (40%), whereas phototrophic taxa are represented by *O. centrocarpum* (~15%) and *Spiniferites frigidus/elongatus* (~5%). From 25 to 10 cm (~1600–~1800 AD) dinocyst assemblages are dominated by the heterotrophic taxa *Brigantedinium* spp and *Echinidinium* spp. (~50 and ~10%, respectively), whereas the relative abundance of *I. minutum* records a sharp decrease (from ~50%–~25%). During this interval phototrophic taxa are mainly represented by *O. centrocarpum* (~10%). These assemblages indicate SSTs (August) close to modern values, whereas the trend suggests a sea-ice cover decrease from 9.5 to 8 months/year accompanied by increased SSSs in the upper part of the core spanning the last two centuries.

Core 004 BC records dinocyst concentrations (Fig. 10) ranging from 1986 to 8066 cysts/cm^3 (average 4872 cysts/cm^3) with the dominance of the two heterotrophic taxa *Brigantedinium* spp. (25%). and *I. minutum* (50%) accompanied by other taxa (*Islandinium*? *cezare*, *E.chinidinium aculeatum*, *Echinidium karaense*, cyst of *Polykrikos* Arctic morphotype). The reconstructed SSTs (August) show a trend towards modern values that is reaches at the top of the core.

5. Discussion

5.1. The gradual break-up of the IIS in the east and central part of the MANWP

The absence of dinocysts together with high $CaCO_3$ (detrital) content, high magnetic susceptibility, high C/N ratio and low $\delta^{13}C$ values at the base of core 009 PC, between 11,100 and 10,800 cal BP (Zone I) indicates that Lancaster Sound site has recorded large terrigenous inputs related to an erosive dynamic during this time interval. Stable isotopes, $CaCO_3$ content and magnetic susceptibility from core 004 PC reveal the same pattern from 10,800 until 8500 cal BP.

The paleolimnological record of diatoms from Prescott Island in the central CAA has shown that diatoms remained absent until 11,000 cal BP, but that high values of carbon content and magnetic susceptibility were probably due to high energy glacial outwash

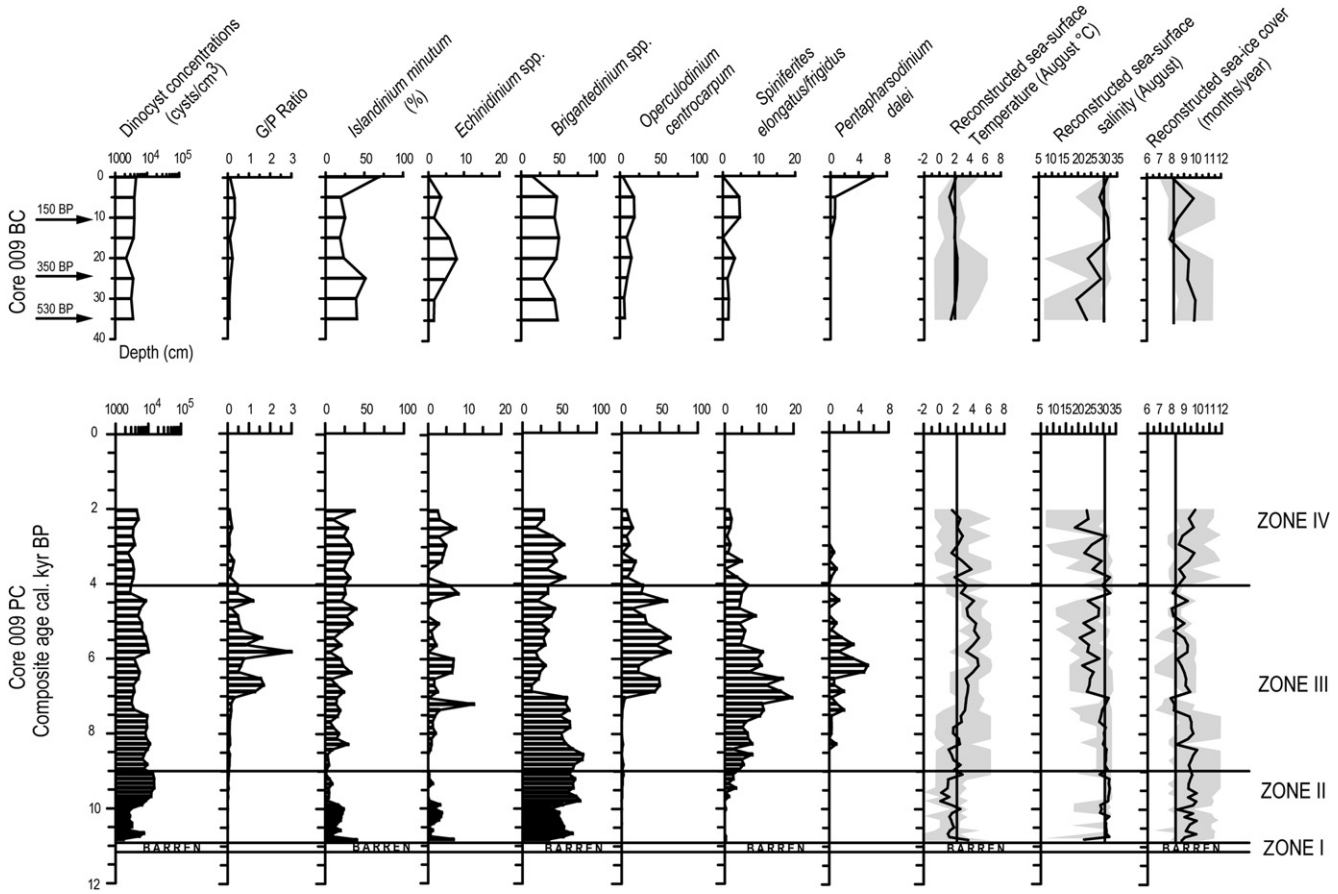

Fig. 9. Diagram of dinocyst concentrations, Gonyaulacales/Peridiniales (G/P ratio), relative abundance of dinocyst taxa and quantitative estimates of sea-surface conditions based on modern analogue technique (MAT) applied to dinocyst assemblages in cores 009 BC and 009 PC. The thick black lines correspond to the best estimates, which are the averages weighted inversely to the distance for the five best modern analogues. The grey zones correspond to the minimum and maximum values possible according to the set of five best analogues. The vertical grey lines indicate the values of modern sea-surface conditions. The chronology of core 009 BC is estimated from ^{210}Pb measurements and was converted from AD to cal BP ages.

(Finkelstein and Gajewski, 2007). Andrews et al. (1995, 1996, 1998), Dyke (2008) and Parnell et al. (2007) have reported detrital carbonate layers in cores from the Northern Baffin Bay, the Labrador Sea and the Northern North Atlantic around 11,000 cal BP. Similarly Scott et al. (2009) observed an IRD rich layer prior to 11,000 cal BP, in a core from the Amundsen Gulf in the western CAA. Recently, Darby and Zimmerman (2008) found in cores from the Fram Strait, central Arctic and Chukchi Borderland six or seven sequences of IRD peaks dated from 36,000 to 11,000 cal BP, which they associate to ice calving and discharge events in the Arctic. The last IRD sequence recorded took place around 11,500 cal BP. This timing is closely related to the first stage of the IIS decay as suggested by England et al. (2000, 2006). Therefore, we associate the large terrigenous inputs at the base of cores 009 and 004 PC to the final collapse of the IIS in the CAA. The high $CaCO_3$ content at the base of both cores probably originates from glacial erosion on Devon Island and Ellesmere Island. The bedrock of this area consists of a Precambrian crystalline basement, overlain by a lower Paleozoic succession dominated by shallow marine platform carbonates (Bischof and Darby, 1999; Parnell et al., 2007). The fact that the central CAA was the center of the maximum Innuitian uplift (maximum former ice thickness reaching more than 1 km) probably explains why Barrow Strait site recorded the Innuitian deglaciation over a much longer time interval.

The occurrence of dinocysts at 10,800 cal BP together with a gradual increase of the C_{org} content and a gradual decrease of both the C/N ratio and detrital carbonate content marked the gradual development of the biological activity in surface waters and the beginning of hemipelagic sedimentation in core 009 PC. It corresponds to zone II, dated between 10,800 and 9000 cal BP, in which quantitative estimates of past sea-surface parameters suggest low SSTs (August) and sea-ice cover for 10 months/year. The harsh reconstructed climatic conditions between 10,800 and 9000 cal BP are consistent with records based on dinocyst, diatoms and foraminifers from northernmost Baffin Bay (Levac et al., 2001; Knudsen et al., 2008). However, it contradicts results based on bowhead bones remains (Dyke et al., 1996) indicating less sea-ice cover in the CAA from 10,600 to 8500 cal BP. Less sea-ice cover ($\sim$1.5 months/year lower than modern conditions) is also indicate by our records from central CAA (Barrow Strait) during that time interval. Recently, based on the IP_{25} biomarker, Vare et al. (2009) also found less sea-ice in central CAA during that time. We associate the reduced ice cover in Barrow Strait with glacial outwash related to the last step of the Innuitian deglaciation triggering high terrigenous inputs as suggested by high magnetic susceptibility values and high detrital carbonate content as well as high C/N ratio. In contrast, the reconstructed harsh sea-surface conditions in Lancaster Sound and northernmost Baffin Bay could be due to the presence of an ice-stream fed by the coalescence of the IIS and GIS (Blake, 1992; Kelly et al., 1999; Zreda et al., 1999; England et al., 2000, 2006). Recently, Dyke (2008) shown that the area of Baffin Bay was marked by active ice-streams between $\sim$10 and 9000 cal BP. Cooler conditions in Lancaster Sound could also be due to limited exchange between the North Atlantic Ocean and Baffin Bay during that time. In modern conditions, the WGC transports polar

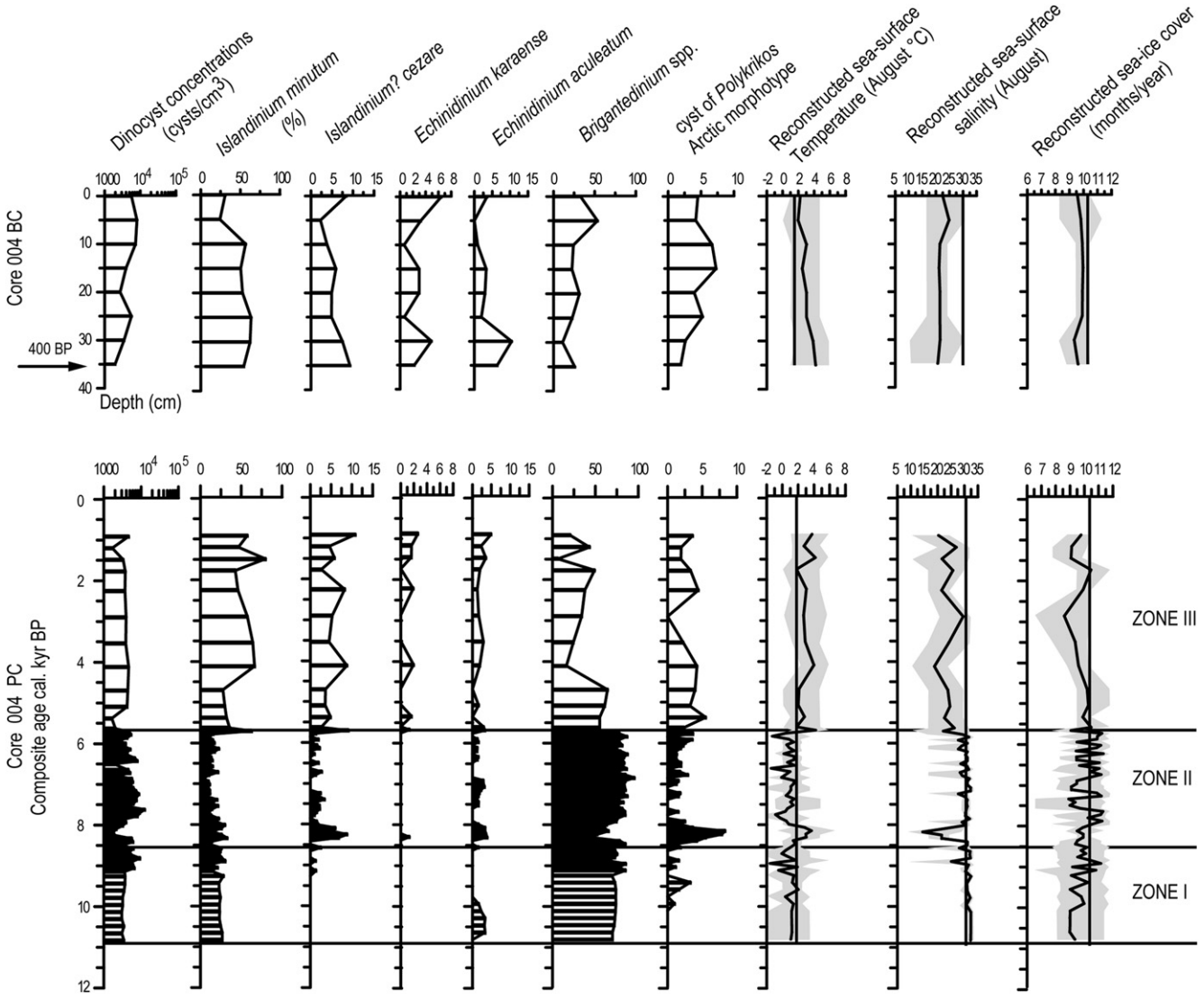

Fig. 10. Diagram of dinocyst concentrations, relative abundance of dinocyst taxa and quantitative estimates of sea-surface conditions based on modern analogue technique (MAT) applied to dinocyst assemblages in cores 004 BC and 004 PC. The thick black lines correspond to the best estimates, which are the averages weighted inversely to the distance for the five best modern analogues. The grey zones correspond to the minimum and maximum values possible according to the set of five best analogues. The vertical grey lines indicate the values of modern sea-surface conditions. The chronology of core 004 BC is estimated from ^{210}Pb measurements and was converted from AD to cal BP ages.

surface water of EGC origin, whereas relatively warm and salty intermediate Atlantic water, originating from the IC, is found between ~200 and 500 m water depth (Cuny et al., 2002). Several works in north and central Baffin Bay have shown that the PML is affected by this warm intermediate Atlantic water through turbulent mixing and upwelling (Knudsen et al., 2008; Zweng and Munchow, 2006; Dunlap and Tang, 2006; Gratton et al., 2003; Ingram et al., 2002; Melling et al., 2001). Based on diatoms, foraminifers and the physical properties of sediments in cores from western Greenland, Ren et al. (2009) and Lloyd et al. (2005) found a weaker WGC before 9000 cal BP. Therefore the reconstructed harsh conditions in Lancaster Sound between 10,800 and 9000 cal BP could be linked to the presence of an ice-stream, a reduced influence of the warm Atlantic water in the area of Baffin Bay or both.

5.2. The early to middle Holocene in the MANWP: major oceanographic changes

The first occurrence of the phototrophic taxa *Spiniferites elongatus/frigidus* around 9000 cal BP in core 009 PC at the transition between zone II and zone III marks the establishment of a gradual warming as suggested by the reconstructed SSTs (August). Maximum SSTs (August, 3 °C above present) were reached between 6000 and 5000 cal BP in zone III, when the phototrophic taxa *O. centrocarpum* and *P. dalei* record their maximum abundance. Based on dinocyst assemblages in cores from Baffin Bay, southwest Greenland and the Laptev Sea, Rochon et al. (2006), Levac et al. (2001), de Vernal and Hillaire-Marcel (2006) and Polyakova et al. (2005) found warmer conditions during the early-middle Holocene. Similarly, diatoms assemblages in cores from the Reykjanes Ridge in the subpolar North Atlantic, Greenland-Iceland-Norwegian seas (GIN seas) and the northern shelf of Iceland indicate an increase influence of warm Atlantic water in the upper water column during the early-middle Holocene (Andersen et al., 2004a, 2004b; Koç and Jansen, 2002; Justwan et al., 2008). Several studies based on mesopelagic and benthic foraminifers in cores from the Barents and Chukchi seas reported a maximum inflow rate of Atlantic water during the early Holocene around 8000 cal BP (Duplessy et al., 2001, 2005; Hillaire-Marcel et al., 2004; de Vernal et al., 2005b). Recently, Ślubowska-Woldengen et al. (2008) using

benthic foraminifers also found an increasing inflow of the warm Atlantic water in the Barents Sea, Svalbard shelf and Iceland shelf accompanied by a strengthening of both the WSC and IC. These are consistent with benthic foraminifers records from west Greenland, which suggest a strengthening of the warm WGC since 9000 cal BP (Lloyd et al., 2005). A strengthening of both the IC and WGC indicates an increase influence of the warm intermediate Atlantic water (Ślubowska-Woldengen et al., 2008). Positive SST anomalies during the early-middle Holocene were found along the main axis of the NAC and NwAC (de Vernal and Hillaire-Marcel, 2006) suggesting a strong influence of the warm intermediate Atlantic water in the upper water column.

Warmer conditions in the eastern Arctic during the early-middle Holocene were also reported from continental records. Based on diatom assemblages from northeast Ellesmere Island lakes, Smith (2002) reported warmer conditions in the early/middle Holocene. Data on stable isotopes from southwestern Greenland (Anderson and Leng, 2004) indicate negative precipitation/evaporation balance during this time interval. Pollen assemblages and concentrations in cores from Baffin Island lakes suggest warmer conditions around 6000 cal BP (Kerwin et al., 2004). Similarly, chironomids from lakes in Baffin Island suggest milder conditions during the middle Holocene (Miller et al., 2005; Francis et al., 2006). $\delta^{18}O$ data in ice core from Devon Island ice cap also indicate warmer conditions during the early-middle Holocene (Fisher, 1976, 1979; Fisher and Koerner, 1980; Fisher et al., 1983).

In contrast, our records from the central CAA (Barrow Strait) show an opposite trend between 8000 and 5500 cal BP with minimum reconstructed SSTs (August, 3 °C lower than present) and variation of sea-ice cover (from 9 to 11 months/year). Dyke et al. (1996) shown that bowheads whales were excluded in the central channels of the CAA between 8500 and 5000 cal BP because of sea-ice conditions more severe than those of historical times. Records based on dinocyst assemblages in cores from the Beaufort and Chukchi seas also indicate extensive sea-ice cover during the early-middle Holocene but with a maximum inflow of warm intermediate Atlantic water (Hillaire-Marcel et al., 2004; de Vernal et al., 2005b; Rochon et al., 2006; McKay et al., 2008). This strong decoupling in the western Arctic between surface layer and the intermediate Atlantic water mass could be due to an increase of Eurasian rivers runoff enhancing a sharp halocline, which promoted the formation of sea-ice. Water in the central CAA is mainly derived from the Canada Basin through M'Clure Strait. The inflow of this low salinity water into the central CAA is consistent with both the decrease of the reconstructed SSSs (August) around 8500 cal BP and the final collapse of the Wellington channel ice-stream, which blocked the full penetration of the Sea until 8500 cal BP (Dyke et al., 2002; England et al., 2006). Strong emergence between 8500 and 7000 cal BP (Dyke, 1998) due to isostatic rebound (~80 m in 1500 years) has also probably triggered variations of the sea-ice cover. Such processes, probably explain the relatively harsh conditions and variations of sea-ice cover recorded in Barrow Strait between 8000 and 5500 cal BP.

Therefore, our records in the eastern and central CAA during the early-middle Holocene (Zone III, Lancaster Sound; Zone II, Barrow Strait) seems to be related to a large scale atmospheric and oceanic reorganization following the last phase of the deglaciation in the Arctic and subarctic areas. In the eastern Arctic, this reorganization was marked by a strong influence of the warm intermediate Atlantic water mass in the upper water column along or near sites influencing by the NAC, NwAC, IC and WGC. The northern Baffin Bay recorded this influence much latter probably due to the gradual strengthening of the WGC after 9000 cal BP that is consistent with major oceanographic changes in the northwestern north Atlantic during the early-middle Holocene (Ren et al., 2009; Knudsen et al., 2008; Hillaire-Marcel et al., 2001). These includes a gradual strengthening of both the IC and the WGC as well as the development of an active site of intermediate Labrador Sea-water formation (Hillaire-Marcel et al., 2001; Lloyd et al., 2005; Knudsen et al., 2008; Ren et al., 2009). In the central and western Arctic, a sharp halocline has promoted the formation of a relatively extensive sea-ice cover. This sharp halocline is probably the result of an increase of Eurasian rivers runoff, which fed the Canada Basin. The inflow of this low salinity water into the central CAA following the last step of the Innuitian deglaciation has probably enhanced harsh conditions. The opposition in marine records between the eastern and western Arctic together with the simultaneous increase in temperatures over land suggests a strong coupling of the oceanic-atmospheric system during this time interval. In modern conditions, such dipole pattern in the Arctic marine realm between the east and west is related to the positive mode of the AO. These include strong divergence in the eastern Arctic leading to positive SST and less summer sea-ice. In western Arctic, strong convergence results in negative SST (Rigor et al., 2002) and relatively extensive sea-ice cover accompanied by an increase in Eurasian rivers discharge due to storm track (Dickson et al., 2000; Peterson et al., 2002; Steele and Ermold, 2004). Therefore, we tentatively associate climate changes in the MANWP from the early to middle Holocene to a possible impact of the AO at the millennial time scale.

5.3. Reverse trend in sea-surface conditions during the middle to late Holocene

From 5500 cal BP to the late Holocene, dinocyst assemblages in core 009 PC show a general decrease in the relative abundance of phototrophic taxa corresponding to the upper part of zone III and zone IV. These are accompanied by a general trend towards relatively low SSTs (August) with values reaching modern conditions (~2 °C) and extensive sea-ice cover (10 months/year). Based on dinocyst, diatoms assemblages and planktonic foraminifers in cores from northernmost Baffin Bay and western Greenland, Levac et al. (2001), Knudsen et al. (2008) and Seidenkrantz et al. (2007, 2008) found cooler conditions in surface water associated with an increasing influence of Arctic water mass during the late Holocene. Similarly, Justwan et al. (2008), Ran et al. (2008) based on diatoms assemblages in core from the North Iceland shelf reported cooler conditions that they associate with a decreasing influence of the warm intermediate Atlantic water in the upper water column together with a reinforcement of the polar water in the EGC during the late Holocene. Increasing influence of polar water in the EGC has been also proposed by Jennings et al. (2002) on the basis of stables isotopes, benthic foramifers and IRD fluxes in cores from east Greenland shelf. A similar decrease in SST was also inferred from alkenones in cores from the North Icelandic shelf (Bendle and Rosell-Melé, 2007) and the Norwegian Sea (Calvo et al., 2002) Based on benthic foraminifers, Lloyd et al. (2007) reported a cooling from 3500 cal BP to the late Holocene in west Greenland. Neoglacial cooling with decreasing Atlantic water influence has been recognized in southwest Greenland on the basis of benthic foraminifers (Lassen et al., 2004; Lloyd et al., 2007). Neoglacial cooling in the eastern Arctic has been also found in many terrestrial records in cores from Ellesmere and Baffin islands and the eastern Arctic as a whole (Michelutti et al., 2006; Wolfe, 2002; Joynt and Wolfe, 2001; Kaufman et al., 2004). A reduction of marine aerosol content and decreasing $\delta^{18}O$ in ice core from Devon Island ice cap suggest increased sea-ice cover and cooling since 3500 cal BP in this area (Bradley, 1990; Fisher et al., 1995, 1983; Fisher, 1976, 1979; Fisher and Koerner, 1980).

In contrast, dinocyst assemblages from Barrow Strait show an increase in species diversity from 5500 cal BP to the late Holocene.

It corresponds to zone III, where quantitative estimates of past sea-surface conditions suggest warmer SSTs (August, ~3 °C warmer than modern conditions) with both a decrease of SSSs and sea-ice cover. Rochon et al. (2006), on the basis of dinocyst assemblages in a sediment core from the Beaufort Sea, found that heterotrophic dinocyst species were gradually replaced by phototrophic taxa, indicating a decrease in sea-ice cover from the middle to late Holocene. Similarly, based on dinocyst assemblages in cores from the Chukchi Sea, McKay et al. (2006, 2008) and de Vernal et al. (2005b) also argued for less sea-ice cover during the late Holocene. Thus, our dinocyst-based reconstructions during the middle to late Holocene with opposite trend between Lancaster Sound and Barrow Strait seem consistent with change in large scale atmospheric pattern such as the AO.

Under modern climate conditions, the AO creates sea-ice dipole pattern between the eastern and western Arctic on annual to decadal time scale. In particular a strong negative mode of the AO enhances less advection of Atlantic water in the Arctic Ocean. This is accompanied by more anticyclonic conditions triggering eastward displacement of the Pacific/Atlantic water front and westward displacement of the transpolar drift along northern Greenland, whereas the Beaufort Gyre is strengthened allowing higher freshwater flux through the CAA (Proshutinsky et al., 2002). During AO^-, divergence in eastern Arctic is reduced resulting in negative SST anomalies. Recently, Darby and Bischof (2004), based on the mineralogy of silt-sand grains from western Arctic cores, have suggested a sea-ice drift pattern analogous to the impact of the AO throughout the Holocene. Therefore, our records from the middle to late Holocene with opposite trends in sea-surface conditions (colder at Lancaster Sound and warmer at Barrow Strait), and marked decreasing SSSs in Barrow Strait (increasing influence of the Beaufort Gyre) could be the result of a shift of the AO mode (from AO^+ in early-middle Holocene to AO^- in middle-late Holocene). Based on driftwood records, Dyke et al. (1997) and Tremblay et al. (1997) found a major switch in the path of the TPD at the onset of middle-late Holocene, which corroborates a change of the AO mode. Comparison of ice core $\delta^{18}O$ record from Devon Island ice cap and the reconstructed SSTs (August) from core 009 suggests a strong atmospheric/oceanic coupling throughout the Holocene in this area (Fig. 11) consistent with the impact of large scale atmospheric pattern such as the Arctic oscillation operating at the millennial time scale.

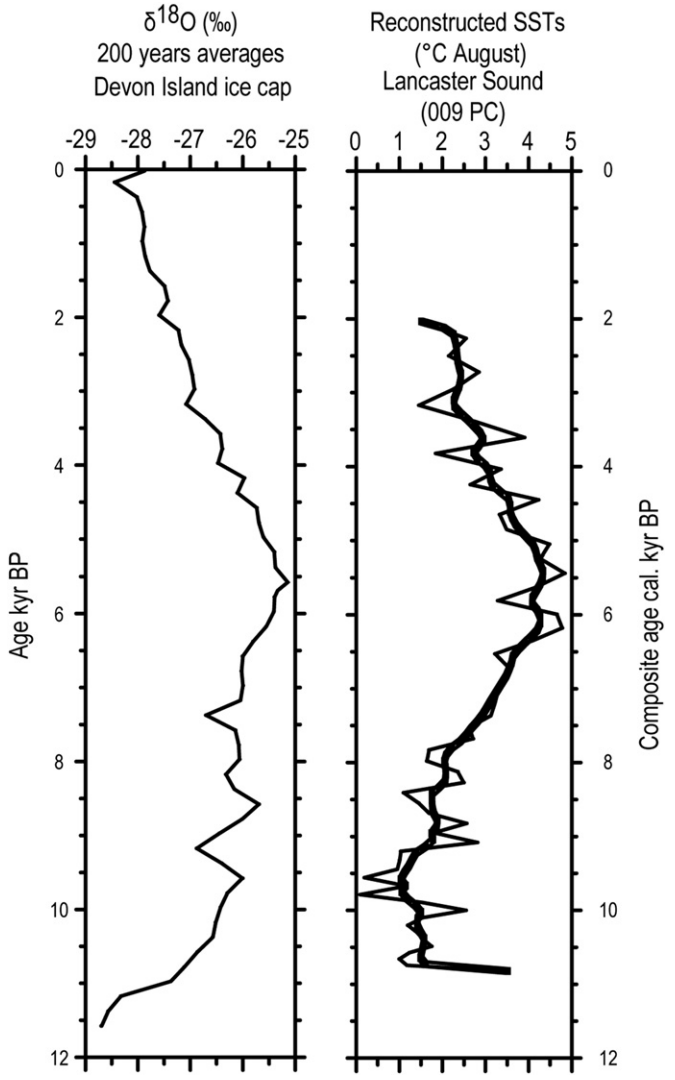

Fig. 11. Holocene ice core $\delta^{18}O$ records from Devon island ice cap (200 years average) vs quantitative estimates of SSTs (August) from Lancaster Sound (core 009 PC). The black thicker line corresponds to a smoothing curve (10 pts) of the reconstructed SST. The comparison of the two diagrams shows the same trend suggesting a strong Oceanic/Atmospheric coupling throughout the Holocene in this area.

5.4. Comparison with previous studies

Our reconstructed sea-ice cover values differ from those derived from the presence of the C_{25} haslene IP_{25} in a nearby sediment core from Barrow Strait (Vare et al., 2009). The presence of IP_{25} in the sediment is indicative of the presence of spring sea-ice (April–May; Vare et al., 2009). Therefore, the flux of IP_{25} provide information on the presence of sea ice for only part of the year. The dinoflagellate-based reconstructions of sea-ice provide the number of months per year where sea-ice covering was higher than 50% and it encompasses the entire year, not just a season. The reconstructed sea-ice values for the present studies (core 004 PC) indicate that between 8.6 and 11.2 months/year had more than 50% of ice coverage (Fig. 10). This means that only a short fraction of the year had less than 50% ice coverage (maximum 3.4 months). According to the set of analogues selected during our computations, the months where sea-ice coverage was <50% are July, August and September. This means that for our entire record our data indicate that the spring sea-ice coverage (April–May), as defined by Vare et al. (2009), was >50% and our method does not allow to quantifying further this value. The major difference between both records lies in the interpretation of the data. Vare et al. (2009) argue that the period from ~10,000 to 3000 cal BP is characterized by less spring sea-ice based on IP_{25} fluxes below the median value, which is used to infer modern conditions. Our reconstructions indicate lower sea-ice conditions (~−0.5−−1.4 month/year) in relation to modern conditions between ~11,000 and 8500 cal BP, and a succession of periods with more (+0.4−+0.9 month/year) and less (−0.3−−1.4 month/year) sea ice between 8500 and ~5500 cal BP. Finally, between 5500 and 3000 cal BP we again reconstruct sea-ice cover values lower than modern conditions (−1.8 month/year). Even though most of our 11,100–3000 cal BP reconstructions indicate less sea-ice cover than modern conditions (with a few exceptions), they are still indicative of relatively harsh conditions similar to those observed today, and they do not suggest more open water conditions as interpreted by Vare et al. (2009). Furthermore, our records indicate a succession of heterotrophic dinoflagellate cyst assemblages over the last ~11,100 cal BP in core 004 PC. Modern dinoflagellate assemblages at the same location in Barrow Strait (A. Rochon unpublished data) are dominated by heterotrophic species of the cyst-forming genus *Protoperidinium* (>90%),

with only 2 non cyst-forming autotrophic species recorded, reflecting the cyst content of the underlying surface sediments.

There are presently no studies available linking the concentration of IP_{25} with the concentration of sea-ice. However, recent field and modeling work on ice algae (Lavoie et al., 2005, 2009, 2010; Rozanska et al., 2009) all suggest that the main factors affecting ice algal biomass (and consequently production of lipidic and aromatic compounds), are light availability (thickness of snow cover, ice thickness) and nutrients availability. Therefore, the abundance and fluxes of the haslene IP_{25}, although indicative of the presence of spring sea-ice, could also reflect the abundance of the biomass rather than sea-ice concentration. This would certainly explain the dominance of heterotrophic taxa in the fossil dinoflagellate cyst assemblages in core 004 PC, since diatoms and ciliates comprise a large part of the heterotrophic dinoflagellate diet (Jacobson, 1999; Jacobson and Anderson, 1986, 1996; Jacobson and Andersen, 1994) However, until a proper calibration exercise is carried out on the abundance of IP_{25} in surface sediments, together with an intercalibration in a multy-proxy study, the comparison of the results of both methods will remain difficult and speculative.

5.5. Historical climate changes

Dinocyst assemblages in core 009 BC are dominated by the two heterotrophic taxa *I. minutum* and *Brigantedinium* spp. throughout the sequence. However, between 25 and 10 cm (from ~AD 1600 to ~AD 1800), the relative abundance of *I. minutum* records a sharp decrease (from 50 to 25%). This is accompanied by an increase in the relative abundance of the heterotrophic taxon *Echinidinium* spp. (from 2% to 10%). During this time interval, quantitative estimates of past sea-surface conditions indicate a trend towards decreasing sea-ice cover (from about 9.5 to 8 months/year) with SSTs (August) slightly warmer than present conditions. From 10 cm to the top of the core (from ~AD 1800 to the beginning of AD 2000), the relative abundance of *I. minutum* increases (from 25% to a maximum value of 75%). The reconstructed SSTs (August) suggest a slight cooling towards modern values. Based on dinocyst assemblages in cores from the Beaufort Sea, Richerol et al. (2008b) also argued for a warming trend from AD 1600 to AD 1800, whereas Levac et al. (2001) suggest a slight cooling of the SSTs during the last 200 years consistent with our records.

Core 004 BC spans approximately the last 400 years, from AD 1600 at the base to the beginning of AD 2000 at the top of the sequence. Dinocyst assemblages are dominated by *I. minutum* and *Brigantedinium* spp. but include occurrence of other taxa such as *Islandinium*? *cezare*, *Echinidinium karaense, E. aculeatum* and the cyst of *Polykrikos* Arctic morphotype. Quantitative estimates of past sea-surface conditions suggest warmer SSTs (August) throughout the sequence with maximum values of 4 °C, which is about 2.5 °C higher than present, at the base of the core (i.e., around AD 1600). A general trend of decreasing temperatures towards modern values is recorded in the uppermost part of the core.

6. Summary and conclusion

Dinocyst assemblages and quantitative estimates of past-surface conditions reveal important climatic change throughout the Holocene in the easternmost and central part of the main axis of the Northwest Passage. During the early Holocene, both sites records high terrigenous inputs as suggested by high C/N ratio, high magnetic susceptibility and high detrital $CaCO_3$ content. This is accompanied in Lancaster Sound by an absence of dinocyst, whereas in Barrow Strait dinocyst assemblages are characterized by low species diversity, *I. minutum* and *Brigantedinium* spp. making up more than 90% of the assemblages. We associate this dynamics with the last stage of the Innuitian deglaciation in this area, which is recorded during ~300 years in Lancaster Sound (from 11,100 to 10,800 cal BP) and during ~2000 years in Barrow Strait (from 10,800 to 8500 cal BP). We explain this delay between the two sites by the presence of the main axis of the Innuitian uplift (zone of maximum thicker ice) following an NE/SW ridge (England et al., 2006) in the north central CAA.

The first occurrence of dinocysts at 10,800 cal BP in Lancaster Sound marked the beginning of the biological productivity in surface waters. From 10,800 to 9000 cal BP dinocyst assemblages were dominated by heterotrophic taxa (*I. minutum* and *Brigantedinium* spp.). This is accompanied by relatively harsh conditions as suggested by quantitative estimates of past sea-surface conditions indicating low SSTs (August) and extensive sea-ice cover (10 months/year). During this time interval, several ice-streams were active in northernmost Baffin Bay, Smith Sound and Kane basins and the WGC and IC were not yet fully established (Ren et al., 2009; Dyke, 2008; England et al., 2006; Olafsdottir et al., 2006; Zreda et al., 1999; Lloyd et al., 2005). Thus, the reconstructed harsh conditions in Lancaster Sound from 10,800 to 9000 cal BP are most likely due to the presence of an active ice-stream together with a limited or absence influence of the warm intermediate Atlantic water mass.

After 8500 cal BP, both sites recorded opposite trends with maximum reconstructed SSTs reached between 6000 and 5000 cal BP (~3 °C more than modern conditions) in Lancaster Sound and minimum SSTs in Barrow Strait around 6000 cal BP (~3 °C lower than modern conditions). These are accompanied by an increase in the relative abundance of phototrophic taxa in Lancaster Sound. We associate the warmer trend in Lancaster Sound with a gradual increase in the influence of the warm intermediate Atlantic water in the upper water column due to the gradual establishment of the WGC. Maximum sea-surface temperatures were also found in cores along or near the WGC, IC, NAC and NwAC (Levac et al., 2001; de Vernal and Hillaire-Marcel, 2006; Ren et al., 2009) during the early-middle Holocene. This was associated with a maximum inflow rate of Atlantic water into the Arctic but with a strong decoupling between the surface layer and the Atlantic water mass in the western Arctic promoting the formation of sea-ice (de Vernal et al., 2005b; Hillaire-Marcel et al., 2004). This sharp halocline in the western Arctic is probably due to an increase of Eurasian rivers runoff, which fed the Canada Basin. The inflow of this low salinity water from the Canada Basin into the central CAA through M'Clure Strait is consistent with the marked decreased of the reconstructed SSSs (August) and the final collapse of the Wellington channel ice-stream around 8500 cal BP (Dyke et al., 2002; England et al., 2006). In modern conditions, such a sea-ice dipole pattern between the eastern and western Arctic accompanied by a maximum inflow of Atlantic water and an increase of Eurasian rivers runoff is closely related to the positive mode of the AO (Dickson et al., 2000; Peterson et al., 2002; Rigor et al., 2002; Steele and Ermold, 2004).

During the late Holocene, the reconstructed sea-surface conditions indicates cooler conditions in Lancaster Sound and warmer conditions in Barrow Strait, suggesting a possible shift of the AO mode (from AO^+ to AO^-) consistent with decreasing SSSs in core 004 PC and changes in driftwood delivered in the CAA (Dyke et al., 1997). At the scale of the Holocene, our records in the central and eastern part of the main axis of the Northwest Passage indicate major oceanographic changes after 8500 cal BP. These major changes are marked by the gradual establishment of the WGC consistent with the onset of an active site of intermediate water formation in the Labrador Sea (Hillaire-Marcel et al., 2001). This large oceanic reorganization following the last deglaciation could have enhanced a strong oceanic/atmospheric coupling as suggested by the comparison of SSTs (August) in Lancaster Sound and $\delta^{18}O$

record from Devon Island ice cap. Therefore, our records seem to confirm the strong coupling between the atmosphere and the ocean in the meridional advection of heat flux from the North Atlantic Ocean to the Arctic Ocean similar to the effect of the Arctic oscillation.

Acknowledgements

This work was funded by the ArcticNet Network of Centres of Excellence and the Natural Science and Engineering Research Council of Canada (NSERC). This is a contribution to the ArcticNet project 1.6, the Polar Climate Stability Network (PCSN) supported by the Canadian Foundation for Climate and Atmospheric Science (CFCAS), and the NSERC-IPY project "International Polar Year: Natural climate variability and forcings in Canadian Arctic and Arctic Ocean – Special Research Opportunity – International Polar Year".

We wish to thank the officers and crew of the CCGS Amundsen for their help and support during sampling. We also wish to express our gratitude to the following people who helped during the collection and analysis of the samples (Robbie Bennett, Bedford Institute of Oceanography, Trecia Schell, DalhousieUniversity, Sylvain Leblanc, Pierre Simard and Guillaume Auclair, UQAR). Thanks are due to Bassam Ghaleb and Jean-François Hélie (GEOTOP) for geochemical and isotope analyses. Discussions with Francesco Barletta (ISMER-GEOTOP) improved this research. We also wish to thank Monika Korte for the CALS7 K.2 inclination data for cores 009 and 004 PC. We are grateful to the two anonymous reviewers for their comments, which helped to improve the manuscript.

References

Andersen, C., Koc, N., Jennings, A., Andrews, J.T., 2004a. Nonuni-form response of the major surface currents in the NordicSeas to insolation forcing: implications for the Holocene climate variability. Paleoceanography 19, PA2003. doi:10.1029/2002PA000873.

Andersen, C., Koç, N., Moros, M., 2004b. A highly unstable Holocene climate in the subpolar North Atlantic: evidence from diatoms. Quaternary Science Reviews 23, 2155–2166.

Anderson, N.J., Leng, M.J., 2004. Increased aridity during the early Holocene in West Greenland inferred from stable isotopes in laminated-lake sediments. 23, 841–849.

Andrews, J.T., Maclean, B., Kerwin, M., Manley, W., Jennings, A.E., Hall, F., 1995. Final stages in the collapse of the laurentide ice sheet, Hudson Strait, Canada, NWT: ^{14}C-AMS dates, seismics stratigraphy, and magnetic susceptibility logs. Quaternary Science Reviews 14, 983–1004.

Andrews, J.T., Osterman, L.E., Jennings, A.E., Syvitski, J.P.M., Miller, G.H., Weiner, N., 1996. Abrupt changes in marine conditions, Sunneshine Fiord, eastern BallinIsland, NWT during the last deglacial transition: Younger Dryas and H-0 events. In: Andrews, J.T., Austin, W.E.N., Bergsten, H., Jennings, A.E. (Eds.), Late Quaternary Palaeoceanography of the North Atlantic Margins. Geological Society Special Publication, pp. 11–27.

Andrews, J.T., Kirby, M.E., Aksu, A., Barber, D.C., Meese, D., 1998. Late quaternary detrital carbonate (DC) layers in baffin bay marine sediments (67°–74°N): correlation with heinrich events in the North Atlantic? Quaternary Science Reviews 17, 1125–1137.

Andrews, J.T., Jennings, A.E., 1990. Geomagnetic secular variations (inclination) of high-latitude Fjord Cores – Eastern Canadian Arctic. Polar Research 8, 245–259.

Appleby, P.G., Oldfield, F., 1983. The assessment of ^{210}Pb data from sites with varying sediment accumulation rates. Hydrobiologia 103, 29–35.

Atkinson, N., England, J., 2004. Postglacial emergence of Amund and Ellef Ringnes islands, Nunavut: implications for the northwest sector of the innuitian ice sheet. Canadian Journal of Earth Sciences 41, 271–283.

Barletta, F., St-Onge, G., Channell, J.E.T., Rochon, A., Polyak, L., Darby, D.A., 2008a. High-resolution paleomagnetic secular variation and relative paleointensity records from the western Canadian Arctic: implication for Holocene stratigraphy and geomagnetic field behaviour. Canadian Journal of Earth Sciences 45, 1265–1281.

Barletta, F., St-Onge, G., Rochon, A., 2008b. Paleomagnetic dating of Holocene Western Canadian Arctic sediments: combined use of secular variation and time-varing spherical harmonic model of the geomagnetic field. In: Arctic Change 2008 Conference Programme and Abstracts, Arctic change 2008, Québec. pp. 177.

Bendle, J.A.P., Rosell-Melé, A., 2007. High-resolution alkenone sea-surface temperature variability on the North Icelandic Shelf: implications for Nordic Seas palaeoclimatic development during the Holocene. The Holocene 17, 9–24.

Besonen, M.R., Patridge, W., Bradley, R.S., Francus, P., Stoner, J.S., Abbott, M.B., 2008. A record of climate over the last millennium based on varved lake sediments from the Canadian High Arctic. The Holocene 18, 169–180.

Bischof, J.F., Darby, D.A., 1999. Quaternary ice transport in the canadian arctic and extent of late Wisconsinan glaciation in the Queen Elizabeth Islands. Canadian Journal of Earth Sciences 36, 2007–2022.

Blake, W.J., 1987. Geological Survey of Canada Radiocarbon Dates XXVI. Geological Survey of Canada, Paper 86–87, 60 pp.

Blake, W.J., 1992. Shell-bearing till along Smith Sound, Ellesmere Island-Greenland: age and significance. In: Robertson, A.-M., Ring-berg, B., Miller, U., Brunnberg, L. (Eds.), Quaternary Stratigraphy, Glacial Morphology and Environmental Change, vol. 81. Sveriges Geologiska Undersokning, pp. 51–58.

Blott, S.J., Pye, K., 2001. GRADISTAT. A grain size distribution and statistics package for the analysis of unconsolidated sediments. Earth and Surface Processes and Landforms 26, 1237–1278.

Bradley, R.S., 1990. Holocene paleoclimatology of the Queen Elizabeth Islands, Canadian high Arctic. Quaternary Science Reviews 9, 365–384.

Breckenridge, A., Johnson, T.C., Beske-Diehl, S., Mothersill, J.S., 2004. The timing of regional Lateglacial events and post-glacial sedimentation rates from Lake Superior. Quaternary Science Reviews 23, 2355–2367.

Calvo, E., Grimalt, J., Jansen, E., 2002. High resolution UK'37sea surface temperature reconstruction in the Norwegian Sea during the Holocene. Quaternary Science Reviews 21, 1385–1394.

Comiso, J.C., Parkinson, C.L., Gersten, R., Stock, L., 2008. Accelerated decline in the Arctic Sea-ice cover. Geophysical Research Letters 35, L01703. doi:10.1029/2007GL031972.

Cuny, J., Rhines, R.B., Niiler, P.P., Bacon, S., 2002. Labrador Sea boundary currents and the fate of the Irminger sea water. Journal of Physical Oceanography 32, 627–647.

Darby, D.A., Bischof, J.F., 2004. A Holocene record of changing Arctic Ocean ice drift analogous to the effects of the Arctic Oscillation. Paleoceanography 19, PA1027. doi:10.1029/2003PA000961.

Darby, D.A., Zimmerman, P., 2008. Ice-rafted detritus events in the Arctic during the last glacial interval, and the timing of the Innuitian and Laurentide Ice Sheet calving events. Polar Research 27, 114–127.

Dickson, R.R., Osborn, T.J., Hurrell, J.W., Meincke, J., Blindheim, J., Adlandsvik, B., Vinje, T., Alekseev, G., Maslows, W., 2000. The Arctic Ocean response to the North Atlantic oscillation. Journal of Climate 13, 2671–2696.

Dickson, R., Rudels, B., Dye, S., Karcher, M., Meincke, J., Yashayaev, I., 2007. Current estimates of freshwater flux through Arctic and subarctic seas. Progress in Oceanography 73, 210–230.

Dukhovskoy, D.S., Johnson, M.A., Proshutinsky, A., 2004. Arctic decadal variability: an auto-oscillatory system of heat and fresh water exchange. Geophysical Research Letters 31, L03302. doi:10.1029/2003GL019023.

Dunlap, E., Tang, C.L., 2006. Modelling the mean circulation of Baffin Bay. Atmosphere-Ocean 44, 99–110.

Duplessy, J.C., Ivanova, E., Murdmaa, I., Paterne, M., Labeyrie, L., 2001. Holocene paleoceanography of the northern Barents Sea and variations of the northward heat transport by the Atlantic Ocean. Boreas 30, 2–16.

Duplessy, J.C., Cortijo, E., Ivanova, E., Khusid, T., Labeyrie, L., Levitan, M., Murdmaa, I., Paterne, M., 2005. Paleoceanography of the Barents Sea during the Holocene. Paleoceanography 20, PA4004. doi:10.1029/2004PA001116.

Dyke, A.S., 1998. Holocene delevelling of Devon Island, Arctic Canada: implications for ice sheet geometry and crustal response. Canadian Journal of Earth Sciences 35, 885–904.

Dyke, A.S., 1999. Last glacial maximum and deglaciation of Devon Island, Arctic Canada: support for an innuitian ice sheet. Quaternary Science Reviews 18, 393–420.

Dyke, A.S., 2008. The Steens by inlet ice-stream in the context of the deglaciation of Northern Baffin Island, Eastern Arctic Canada. Earth Surface Processes and Landforms 33, 573–592.

Dyke, A.S., England, J., 2003. Canada's most northerly postglacial bowhead whales (Balaena mysticetus): Holocene sea-ice conditions and polynya development. Arctic 56, 14–20.

Dyke, A.S., Hooper, J., Savelle, J.M., 1996. A history of sea-ice in the Canadian Arctic Archipelago based on postglacial remains of the bowhead whale (Balaena mysticetus). Arctic 49, 235–255.

Dyke, A.S., England, J., Reimnitz, E., Jette, H., 1997. Changes in driftwood delivery to the Canadian arctic archipelago: the hypothesis of postglacial oscillations of the transpolar drift. Arctic 50, 1–16.

Dyke, A.S., Andrews, J.T., Clark, P.U., England, J.H., Miller, G.H., Shaw, J., Veillette, J.J., 2002. The laurentide and innuitian ice sheets during the last glacial maximum. Quaternary Science Reviews 21, 9–31.

England, J., 1998. Support for the innuitian ice sheet in the Canadian high Arctic during the last glacial maximum. Journal of Quaternary Science 13, 275–280.

England, J., 1999. Coalescent Greenland and innuitian ice during the last glacial maximum: revising the Quaternary of the Canadian high Arctic. Quaternary Science Reviews 18, 421–456.

England, J., Smith, I.R., Evans, D.J.A., 2000. The last glaciation of east-central Ellesmere Island, Nunavut: ice dynamics, deglacial chronology, and sea level change. Canadian Journal of Earth Sciences 37, 1355–1371.

England, J., Atkinson, N., Dyke, A., Evans, D., Zreda, M., 2004. Late wisconsinan buildup and wastage of the innuitian Ice Sheet across southern Ellesmere Island, Nunavut. Canadian Journal of Earth Sciences 41, 39–61.

England, J., Atkinson, N., Bednarski, J., Dyke, A.S., Hodgson, D.A., Cofaigh, C.O., 2006. The Innuitian Ice Sheet: configuration, dynamics and chronology. Quaternary Science Reviews 25, 689–703.

England, J., Lajeunesse, P., 2004. Overview of the Innutian Ice Sheet and New Perspectives on Episodic Ice Shelves on the NW Laurentide Ice Sheet. In: 49th Annual Meeting of the Geological Association of Canada and the Mineralogical Association of Canada. Brock University, St. Catharines, Ontario.

Finkelstein, S.A., Gaiewski, K., 2007. A palaeolimnological record of diatom community dynamics and late-Holocene climatic changes from Prescott Island, Nunavut, central Canadian Arctic. The Holocene 17, 803–812.

Finkelstein, S.A., Gajewski, K., 2008. Responses of Fragilarioid-dominated diatom assemblages in a small Arctic lake to Holocene climatic changes, Russell Island, Nunavut, Canada. Journal of Paleolimnology 40, 1079–1095.

Fisher, D.A., 1976. "A Study of Two O-18 Records From Devon Ice Cap, Canada, and Comparison of them to Camp Century O-18 record, Greenland." Ph.D. thesis, University of Copenhagen. 278 pp.

Fisher, D.A., 1979. Comparison of 105 years of oxygen isotope and insoluble impurity profiles from the Devon Island and Camp Century ice cores. Quaternary Research 11, 299–305.

Fisher, D.A., Koerner, R.M., Paterson, W.S.B., Dansgaard, W., Gundestrup, N., Reeh, N., 1983. Effect of wind scouring on climatic records from ice-core oxygen-isotope profiles. Nature 301, 205–209.

Fisher, D.A., Koerner, R.M., Reeh, N., 1995. Holocene climatic records from Agassiz ice cap, Ellesmere Island, Nwt, Canada. The Holocene 5, 19–24.

Fisher, D., Dyke, A., Koerner, R., Bourgeois, J., Kinnard, C., Zdanowicz, C., de Vernal, A., Hillaire-Marcel, C., Savelle, J., Rochon, A., 2006. Natural variability of Arctic sea–ice over the Holocene. Eos 87, 273–280.

Fisher, D.A., Koerner, R.M., 1980. Some aspects of climatic change in the High Arctic during the Holocene as deduced from ice cores. In: Mahaney, W.C. (Ed.), Quaternary Climatic Change Symposium. York University, Toronto, pp. 349–371.

Francis, D.R., Wolfe, A.P., Walker, I.R., Miller, G.H., 2006. Interglacial and Holocene temperature reconstructions based on midge remains in sediments of two lakes from Baffin Island, Nunavut, Arctic Canada. Palaeogeography, Palaeoclimatology, Palaeoecology 236, 107–124.

Gajewski, K., Bouchard, G., Wilson, S., Kurek, J., Cwynar, L., 2005. Distribution of Chironomidae (Insecta: Diptera) head capsules in recent sediments of Canadian Arctic lakes. Hydrobiologia 549, 131–143.

Geiss, C.E., Banerjee, S.K., 2003. A Holocene–Late Pleistocene geomagnetic inclination record from Grandfather Lake, SW Alaska. Geophysic Journal International 153, 497–507.

Golubeva, E.N., Platov, G.A., 2007. On improving the simulation of Atlantic water circulation in the Arctic ocean. Journal of Geophysical Research 112, C04S05. doi:10.1029/2006JC003734.

Gratton, Y., Mellimg, H., Ingram, R.G., Rail, M.E., 2003. Circulation and formation of the North Water Polynya, Baffin Bay. Geophysical Research Abstracts 5, 08068.

Guiot, J., Goeury, C., 1996. Pppbase, a software for statistical analysis of paleoecological and paleoclimatological data. Dendrochronologia 14, 295–300.

Guiot, J., de Vernal, A., 2007. Transfer functions: methods for quantitative paleoceanography based on microfossils. In: Hillaire-Marcel, de Vernal (Eds.), Proxies in Late Cenozoic Paleoceanography. Elsevier, pp. 523–563.

Hamel, D., de Vernal, A., Gosselin, M., Hillaire-Marcel, C., 2002. Organic-walled microfossils and geochemical tracers: sedimentary indicators of productivity changes in the North Water and northern Baffin Bay during the last centuries. Deep-Sea Research Part II-Topical Studies in Oceanography 49, 5277–5295.

Head, M.J., Harland, R., Matthiessen, J., 2001. Cold marine indicators of the late Quaternary: the new dinoflagellate cyst genus *Islandinium* and related morphotypes. Journal of Quaternary Science 16, 621–636.

Hillaire-Marcel, C., de Vernal, A., Bilodeau, G., Weaver, A.J., 2001. Absence of deep-water formation in the Labrador Sea during the last interglacial period. Nature 410, 1073–1077.

Hillaire-Marcel, C., de Vernal, A., Polyak, L., Darby, D., 2004. Size-dependent isotopic composition of planktic foraminifers from Chukchi Sea vs. NW Atlantic sediments – implications for the Holocene paleoceanography of the western Arctic. Quaternary Science Reviews 23, 245–260.

Howell, S.E.L., Duguay, C.R., Markus, T., 2009. Sea-ice conditions and melt season duration variability within the Canadian Arctic Archipelago: 1979–2008. Geophysical Research Letters 36, L10502. doi:10.1029/2009GL037681.

Hughen, K.A., Baillie, M.G.L., Bard, E., Bayliss, A., Beck, J.W., Blackwell, P.G., Buck, C.E., Burr, G.S., Cutler, K.B., Damon, P.E., Edwards, R.L., Fairbanks, R.G., Friedrich, M., Guilderson, T.P., Herring, C., Kromer, B., McCormac, F.G., Manning, S.W., Ramsey, C.B., Reimer, P.J., Reimer, R.W., Remmele, S., Southon, J.R., Stuiver, M., Talamo, S., Taylor, F.W., van der Plicht, J., Weyhenmeyer, C.E., 2004. Marine04 Marine radiocarbon age calibration, 26–0 ka BP. Radiocarbon 46, 1059–1086.

Ingram, R.G., Bâcle, J., Barber, D.G., Gratton, Y., Melling, H., 2002. An overview of physical processes in the North Water. DeepSea Research II 49, 4893–4906.

Intergovernmental Panel on Climate Change, 2007. Climate change 2007: synthesis report. Contribution of working groups I, II and III to the fourth assessment report of the Intergovernmental Panel on Climate Change. Core Writing Team. In: Pachauri, R.K., Reisinger, A. (Eds.). IPCC, Geneva, Switzerland, p. 104.

Jacobson, D.M., 1999. A brief history of dinoflagellate feeding research. Journal of Eukaryotic Microbiology 46, 376–381.

Jacobson, D.M., Andersen, R.A., 1994. The discovery and mixotrophy in photosynthetic species of Dinophysis (Dinophyceae): light and electron microscopical observations of food vacuoles in *Dinophysis acuminata, D. norvegica* and two heterotrophic dinophysoid dinoflagellates. Phycologia 33, 97–110.

Jacobson, D.M., Anderson, D.M., 1986. The cate heterotrophic dinoflagellates: feeding behaviour and mechanisms. Journal of Phycology 22, 249–258.

Jacobson, D.M., Anderson, D.M., 1996. Widespread phagocytosis of ciliates and other protists by marine mixotrophic and heterotrophic the cate dinoflagellates. Journal of Phycology 32, 279–285.

Jakobsson, M., 2002. Hypsometry and volume of the Arctic Ocean and its constituent seas. Geochemistry Geophysics Geosystems 3, 1028. doi:10.1029/2001GC000302.

Jakobsson, M., 2004. Correction to "hypsometry and volume of the Arctic Ocean and its constituent seas". Geochemistry Geophysics Geosystems 5, Q02005. doi:10.1029/2004GC000694.

Jennings, A.E., Knudsen, K.L., Hald, M., Hansen, C.V., Andrews, J.T., 2002. A mid-Holocene shift in Arctic sea-ice variability on the East Greenland Shelf. The Holocene 12, 49–58.

Johnson, M.A., Proshutinsky, A.Y., Polyakov, I.V., 1999. Atmospheric patterns forcing two regimes of arctic circulation: a return to anticyclonic conditions? Geophysical Research Letters 26, 1621–1624.

Jones, E.P., 2001. Circulation in the Arctic Ocean. Polar Reasearch 20, 139–146.

Jones, E.P., Swift, J.H., Anderson, L.G., Lipizer, M., Civitarese, G., Falkner, K.K., Kattner, G., McLaughlin, F., 2003. Tracing Pacific water in the North Atlantic Ocean. Journal of Geophysical Research-Oceans 108 (C4), 3116. doi:10.1029/2001JC001141.

Joynt III, E.H., Wolfe, A.P., 2001. Paleoenvironmental inference models from sediment diatom assemblages in Baffin Island lakes (Nunavut, Canada) and reconstruction of summer water temperature. Canadian Journal of Fisheries and Aquatic Sciences 58, 1222–1243.

Justwan, A., Koc, N., Jennings, A.E., 2008. Evolution of the Irminger and East Icelandic Current systems through the Holocene, revealed by diatom-based sea-surface temperature reconstructions. Quaternary Science Reviews 27, 1571–1582.

Kaufman, D.S., Ager, T.A., Anderson, N.J., Anderson, P.M., Andrews, J.T., Bartlein, P.J., Brubaker, L.B., Coats, L.L., Cwynar, L.C., Duvall, M.L., Dyke, A.S., Edwards, M.E., Eisner, W.R., Gajewski, K., Geirsdóttir, A., Hu, F.S., Jennings, A.E., Kaplan, M.R., Kerwin, M.W., Lozhkin, A.V., MacDonald, G.M., Miller, G.H., Mock, C.J., Oswald, W.W., Otto-Bliesner, B.L., Porinchu, D.F., Rühland, K., Smol, J.P., Steig, E.J., Wolfe, B.B., 2004. Holocene thermal maximum in the western Arctic (0–180°W). Quaternary Science Reviews 23, 529–560.

Kelly, M., Funder, S., Houmark-Nielsen, M., Knudsen, K.L., Kronborg, C., Landvik, J., Sorby, L., 1999. Quaternary glacial and marine environmental history of northwest Greenland: a review and reappraisal. Quaternary Science Reviews 18, 373–392.

Kerwin, M.W., Overpeck, J.T., Webb, R.S., Anderson, K.H., 2004. Pollen-based summer temperature reconstructions for the eastern Canadian boreal forest, subarctic, and Arctic. Quaternary Science Reviews 23, 1901–1924.

Kirschvink, J.L., 1980. The least-squares line and plane and the analysis of paleomagnetic data. Geophysical Journal of the Royal Astronomical Society 62, 699–718.

Knudsen, K.L., Stabell, B., Seidenkrantz, M.-S., Eirıksson, J., Blake Jr., W., 2008. Deglacial and Holocene conditions in northernmost Baffin Bay: sediments, foraminifera, diatoms and stable isotopes. Boreas 37, 346–376.

Kokinos, J.P., Eglinton, T.I., Goni, M.A., Boon, J.J., Martoglio, P.A., Anderson, D.M., 1998. Characterization of a highly resistant biomacromolecular material in the cell wall of a marine dinoflagellate resting cyst. Organic Geochemistry 28, 265–288.

Korte, M., Constable, C.G., 2005. Continuous geomagnetic field models for the past 7 millennia: 2. CALS7K. Geochemistry Geophysics Geosystems 6, Q02H16. doi:10.1029/2004GC000801.

Korte, M., Genevey, A., Constable, C.G., Frank, U., Schnepp, E., 2005. Continuous geomagnetic field models for the past 7 millennia: 1. A new global data compilation. Geochemistry Geophysics Geosystems 6, Q02H15. doi:10.1029/2004GC000800.

Kotilainen, A.T., Saarinen, T., Winterhalter, B., 2000. High-resolution paleomagnetic dating of sediments deposited in the central Baltic Sea during the last 3000 years. Marine Geology 166, 51–64.

Koç, N., Jansen, E., 2002. Holocene climate evolution of the North Atlantic Ocean and the NordicSeas – a synthesis of new results. In: Wefer (Ed.), Climate and History in the North Atlantic Realm. Springer-Verlag, Berlin Heidelberg, pp. 165–173.

Kunz-Pirrung, M., 1998. Rekonstruktion der Oberflächenwassermassen der östlichen Laptevsee im Holozän anhand von aquatischen Palynomorphen. Berichte Zur Polarforschung 281, 117.

Kunz-Pirrung, M., 2001. Dinoflagellate cyst assemblages in surface sediments of the Laptev Sea region (Arctic Ocean) and their relationship to hydrographic conditions. Journal of Quaternary Science 16, 637–649.

Kunz-Pirrung, M., Matthiessen, J., de Vernal, A., 2001. Late Holocene dinoflagellate cysts as indicators for short-term climate variability in the eastern Laptev Sea (Arctic Ocean). Journal of Quaternary Science 16, 711–716.

Lassen, S.J., Kuijpers, A., Kunzendorf, H., Hoffmann-Wieck, G., Mikkelsen, N., Konradi, P., 2004. Late-Holocene Atlantic bottom-water variability in Igaliku

Fjord, South Greenland, reconstructed from foraminifera faunas. Holocene 14, 165–171.
Lavoie, D., Denman, K., Michel, C., 2005. Modeling ice algal growth and decline in a seasonally ice-covered region of the Arctic (resolute Passage, Canadian Archipelago). Journal of Geophysical Research 110, C11009. doi:10.1029/2005JC002922.
Lavoie, D., Macdonald, R.W., Denman, K., 2009. Primary productivity and export fluxes on the Canadian Shelf of the Beaufort Sea: a modelling study. Journal of Marine Systems 75, 17–32.
Lavoie, D., Denman, K.L., Macdonald, R.W., 2010. Effects of future climate change on primary productivity and export fluxes in the Beaufort Sea. Journal of Geophysical Research 115, C04018. doi:10.1029/2009JC005493, 15 pp.
Ledu, D., Rochon, A., de Vernal, A., St-Onge, G., 2007. Palynological Evidence of the Holocene Thermal Maximum in the Northwest Passage: a Possible Shift in the Arctic Oscillation at the Millennial Time Scale. 4th Arctic Net Annual Scientific Meeting, Program and Abstracts, 65, Collingwood, Ontario, Canada.
Ledu, D., Rochon, A., de Vernal, A., St-Onge, G., 2008. Palynological evidence of Holocene climate changes in the Eastern Arctic: a possible influence of the Arctic oscillation at the millennial time scale. Canadian Journal of Earth Science 45, 1363–1375.
Levac, E., de Vernal, A., Blake, W., 2001. Sea-surface conditions in northernmost Baffin Bay during the Holocene: palynological evidence. Journal of Quaternary Science 16, 353–363.
Lisé-Pronovost, A., St-Onge, G., Brachfeld, S., Bareletta, F., Darby, D., 2009. Paleomagnetic constraints on the Holocene stratigraphy of the Arctic Alaskan margin. Global and Planetary Change 68, 85–99. doi:10.1016/j.gloplacha.2009.03.015.
Lloyd, J.M., Park, L.A., Kuijpers, A., Moros, M., 2005. Early Holocene palaeoceanography and deglacial chronology of Disko Bugt, west Greenland. Quaternary Science Reviews 24, 1741–1755.
Lloyd, J.M., Kuijpers, A., Long, A., Moros, M., Park, L.A., 2007. Foraminiferal reconstruction of mid- to late-Holocene ocean circulation and climate variability in Disko Bugt, West Greenland. The Holocene 17, 1079–1091.
Mangerud, J., Gulliksen, S., 1975. Apparent radioacarbon ages of recent marine shells from Norway, Spitsbergen and Arctic Canada. Quaternary Research 5, 263–273.
Marret, F., Zonneveld, K.A.F., 2003. Atlas of modern organic-walled dinoflagellate cyst distribution. Review of Palaeobotany and Palynology 125, 1–200.
Matthews, J., 1969. The assessment of a method for the determination of absolute pollen frequencies. New Phytologist 68, 161–166.
Mazaud, A., 2005. User-friendly software for vector analysis of the magnetization of long sediment cores. Geochemistry Geophysics Geosystems 6, Q12006. doi:10.1029/2005GC001036.
McKay, J.L., Hillaire-Marcel, C., de Vernal, A., Polyak, L., Darby, D., 2006. Holocene paleoceanography of the Chukchi Sea/Alaskan margin, western Arctic Ocean. In: American Geophysical Union, Fall Meeting 2006. AGU, San Francisco, USA.
McKay, J.L., de Vernal, A., Hillaire-Marcel, C., Not, C., Polyak, L., Darby, D., 2008. Holocene fluctuations in Arctic sea-ice cover: dinocyst-based reconstructions for the eastern Chukchi Sea. Canadian Journal of Earth Science 45, 1377–1397.
McLaughlin, F.A., Carmack, E.C., Macdonald, R.W., Melling, H., Swift, J.H., Wheeler, P.A., Sherr, B.F., Sherr, E.B., 2004. The joint roles of Pacific and Atlantic-origin waters in the Canada Basin, 1997-1998. Deep-Sea Research Part I-Oceanographic Research Papers 51, 107–128.
Melling, H., 2002. Sea-ice of the northern Canadian Arctic archipelago. Journal of Geophysical Research-Oceans 107 (C11), 3181. doi:10.1029/2001JC001102.
Melling, H., Gratton, Y., Ingram, G., 2001. Ocean circulation within the North Water Polynya of Baffin Bay. Atmosphere-Ocean 39, 301–325.
Michelutti, N., Douglas, M.S.V., Wolfe, A.P., Smol, J.P., 2006. Heightened sensitivity of a poorly buffered high arctic lake to late-Holocene climatic change. Quaternary Research 65, 421–430.
Miller, G.H., Wolfe, A.P., Briner, J.P., Sauer, P.E., Nesje, A., 2005. Holocene glaciation and climate evolution of Baffin Island, Arctic Canada. Quaternary Science Reviews 24, 1703–1721.
Mudie, P.J., Rochon, A., Levac, E., 2005. Decadal-scale sea-ice changes in the Canadian Arctic and their impacts on humans during the past 4000 years. Environmental Archeologist 10, 113–126.
Mudie, P.J., Rochon, A., Prins, M.A., Soenarjo, D., Troelstra, S.R., Levac, E., Scott, D.B., Roncaglia, L., Kuijpers, A., 2006. Late Pleistocene–Holocene marine geology of Nares Strait region: paleoceanography from foraminifera and dinoflagellate cysts, sedimentology and stable isotopes. Polarforschung 74, 169–183.
Mudie, P.J., Rochon, A., 2001. Distribution of dinoflagellate cysts in the Canadian Arctic marine region. Journal of Quaternary Science 16, 603–620.
National Oceanography Data Center (NODC), WorldOcean Atlas, 2001. National Oceanic and Atmospheric Administration (NOAA). Available from: http://www.nodc.noaa.gov/OC5/WOD01/pr_wod01.html (accessed 01.09.).
National Snow and IceData Center (NSIDC), 1953–2000 [online]. Available from. http://nsidc.org/ (accessed 09.08.).
Olafsdottir, S., Geirsdottir, A., Jennings, A.E., Stoner, J.S., Miller, G.H., 2006. High-resolution Holocene paleoceanographic and paleoclimatic records from Iceland: land sea correlation. American Geophysical Union. Fall Meeting, Abstract#PP43A-1222.
Parnell, J., Bowden, S., Andrews, J.T., Taylor, C., 2007. Biomarker determination as a provenance tool for detrital carbonate events (Heinrich events?): Fingerprinting Quaternary glacial sources into Baffin Bay. Earth and Planetary Science Letters 257, 71–82.
Peterson, B.J., Holmes, R.M., McClelland, J.W., Vörösmarty, C.J., Lammers, R.B., Shiklomanov, A.I., Shoklimanov, I.A., Rahmstorf, S., 2002. Increasing River discharge to the Arctic Ocean. Science 298, 2171–2173.
Podritske, B., Gajewski, K., 2007. Diatom community response to multiple scales of Holocene climate variability in a small lake on Victoria Island, NWT, Canada. Quaternary Science Reviews 26, 3179–3196.
Polyakov, I.V., Alekseev, G.V., Timokhov, L.A., Bhatt, U.S., Colony, R.L., Simmons, H.L., Walsh, D., Walsh, J.E., Zakharov, V.F., 2004. Variability of the intermediate Atlantic water of the Arctic Ocean over the last 100 years. Journal of Climate 17, 4485–4497.
Polyakov, I.V., Johnson, M.A., 2000. Arctic decadal and interdecadal variability. Geophysical Research Letters 27, 4097–4100.
Polyakova, Y.I., Bauch, H.A., Klyuvitkina, T.S., 2005. Early to middle Holocene changes in Laptev Sea water masses deduced from diatom and aquatic palynomorph assemblages. Global and Planetary Change 48, 208–222.
Prinsenberg, S.J., Bennett, E.B., 1987. Mixing and transports in Barrow Strait, the central part of the Northwest passage. Continental Shelf Research 7, 913–935.
Prinsenberg, S.J., Hamilton, J., 2005. Monitoring the volume, freshwater and heat fluxes passing through Lancaster Sound in the Canadian Arctic Archipelago. Atmosphere-Ocean 43, 1–22.
Proshutinsky, A., Bourke, R.H., McLaughlin, F.A., 2002. The role of the Beaufort Gyre in Arctic climate variability: seasonal to decadal climate scales. Geophysical Research Letters 29 (23), 2100. doi:10.1029/2002GL015847.
Proshutinsky, A.Y., Johnson, M.A., 1997. Two circulation regimes of the wind driven Arctic Ocean. Journal of Geophysical Research-Oceans 102, 12493–12514.
Radi, T., de Vernal, A., Peyron, O., 2001. Relationships between dinoflagellate cyst assemblages in surface sediment and hydrographic conditions in the Bering and Chukchi seas. Journal of Quaternary Science 16, 667–680.
Radi, T., de Vernal, A., 2008. Dinocysts as proxy of primary productivity in mid-high latitudes of the Northern Hemisphere. Marine Micropaleontology 68, 84–114.
Ran, L., Jiang, H., Knudsen, K.L., Eiríksson, J., 2008. The mid to late Holocene paleoceanographic changes in the northern North Atlantic. Frontiers of Earth Science in China 2, 449–457.
Ren, J., Jiang, H., Seideinkrantz, M.S., Kuijpers, A., 2009. A diatom-based reconstruction of Early Holocene hydrographic and climatic change in a southwest Greenland fjord. Marine Micropaleontology 70, 166–176.
Richerol, T., Rochon, A., Blasco, S., Scott, D.B., Schell, T.M., Bennett, R.J., 2008a. Distribution of dinoflagellate cysts in surface sediments of the Mackenzie shelf and Amundsen Gulf, Beaufort Sea (Canada). Journal of Marine Systems 74, 825–839.
Richerol, T., Rochon, A., Blasco, S., Scott, D.B., Schell, T.M., Bennett, R.J., 2008b. Evolution of paleo sea-surface conditions over the last 600 years in the Mackenzie Trough, Beaufort Sea (Canada). Marine Micropaleontology 68, 6–20.
Rigor, I.G., Wallace, J.M., Colony, R.L., 2002. Response of sea-ice to the Arctic oscillation. Journal of Climate 15, 2648–2663.
Rochon, A., de Vernal, A., Turon, J.-L., Matthiessen, J., Head, M.J., 1999. Distribution of Recent Dinoflagellate Cysts in Surface Sediments from the North Atlantic and Adjacent Seas, and Quantitative Reconstruction of Sea-surface Parameters. In: Contribution Series, vol. 35. American Association of Stratigraphic Palynologists, 152 pp.
Rochon, A., Scott, D.B., Schell, T.M., Blasco, S., Bennett, R., Mudie, P., 2006. Evolution of sea-surface conditions during the Holocene: comparison between eastern (Baffin Bay and Hudson Strait) and western (Beaufort Sea) Canadian Arctic. In: American Geophysical Union (AGU) Fall Meeting Supplement. pp. 52, San Francisco, USA.
Rochon, A., de Vernal, A., 1994. Palynomorph distribution in recent sediments from the Labrador Sea. Canadian Journal of Earth Sciences 31, 115–127.
Rolland, N., Larocque, I., Francus, P., Pienitz, R., Laperriere, L., 2008. Holocene climate inferred from biological (Diptera: Chironomidae) analyses in a Southampton island (Nunavut, Canada) lake. The Holocene 18, 229–241.
Rózanska, M., Gosselin, M., Poulin, M., Wiktor, J.M., Michel, C., 2009. Influence of environmental factors on the development of bottom ice protist communities during the winter–spring transition. Marine Ecology Progress 386, 43–59. doi:10.3354/meps08092.
Rudels, B., Jones, E.P., Anderson, L.G., Kattner, G., 1994. On the intermediate depth waters of the Arctic Ocean. In: Johannessen, O.M. (Ed.), The Role of Polar Oceans in Shaping the Global Climate. American Geophysical Union, Washington, D.C, pp. 33–46.
Rudels, B., Friedrich, H.J., Quadfasel, D., 1999. The arctic circumpolar boundary current. Deep-Sea Research Part II 46, 1023–1062.
Saarinen, T., 1998. High-resolution palaeosecular variation in northern Europe during the last 3200 years. Physics of the Earth and Planetary Interiors 106, 299–309.
Saarinen, T., 1999. Palaeomagnetic dating of late Holocene sediments in Fennoscandia. Quaternary Science Reviews 18, 889–897.
Savelle, J.M., Dyke, A.S., McCartney, A.P., 2000. Holocene bowhead whale (Balaena mysticetus) mortality patterns in the Canadian Arctic Archipelago. Arctic 53 (4), 414–421.
Schell, T.M., Moss, T.J., Scott, D.B., Rochon, A., 2008. Paleo-sea-ice conditions of the Amundsen Gulf, Canadian Arctic Archipelago: implications from the foraminiferal record of the last 200 years. Journal of Geophysical Research-Oceans 113, C03S02. doi:10.1029/2007JC004202.
Scott, D.B., Schell, T., St-Onge, G., Rochon, A., Blasco, S., 2009. Foraminiferal assemblage changes over the last 15,000 years on the Mackenzie/Beaufort Sea

slope and Amundsen Gulf, Canada: implication for past sea-ice conditions. Paleoceanography 24, PA2219. doi:10.1029/2007PA001575.
Seidenkrantz, M.S., Aagaard-Sørensen, S., Sulsbrück, H., Kuijpers, A., Jensen, K.G., Kunzendorf, H., 2007. Hydrography and climate of the last 4400 years in a SW Greenland fjord: implications for Labrador Sea palaeoceanography. The Holocene 17, 387–401.
Seidenkrantz, M.-S., Roncaglia, L., Fischel, A., Heilmann-Clausen, C., Kuijpers, A., Moros, M., 2008. Variable North Atlantic climate seesaw patterns documented by a late Holocene marine record from Disko Bugt, West Greenland. Marine Micropaleontology 68, 66–83.
Ślubowska-Woldengen, M., Koc, N., Rasmussen, T.L., Klitgaard-Kristensen, D., Hald, M., Jennings, A.E., 2008. Time-slice reconstructions of ocean circulation changes on the continental shelf in the Nordic and Barents Seas during the last 16,000 cal yr BP. Quaternary Science Reviews 27, 1476–1492.
Smith, I.R., 2002. Diatom-based holocene paleoenvironmental records from continental sites on northeastern Ellesmere Island, high Arctic, Canada. Journal of Paleolimnology 27, 9–28.
Snowball, I., Zillén, L., Ojala, A., Saarinen, T., Sandgren, P., 2007. FENNOSTACK and FENNORPIS: varve dated Holocene palaeomagnetic secular variation and relative palaeointensity stacks for Fennoscandia. Erath and Planetary Science Letters 255, 106–116.
Snowball, I., Sandgren, P., 2002. Geomagnetic field variations in northern Sweden during the Holocene quantified from varved lake sediments and their implications for cosmogenic nuclide production rates. Holocene 12, 517–530.
St-Onge, G., Stoner, J.S., Hillaire-Marcel, C., 2003. Holocene paleomagnetic records from the St. Lawrence Estuary, eastern Canada: centennial- to millennial-scale geomagnetic modulation of cosmogenic isotopes. Earth and Planetary Science Letters 209, 113–130.
St-Onge, G., Mulder, T., Piper, D.J.W., Hillaire-Marcel, C., Stoner, J.S., 2004. Earthquake and flood-induced turbidites in the Saguenay Fjord (Québec): a Holocene paleoseismicity record. Quaternary Science Reviews 23, 283–294.
Steele, M., Boyd, T., 1998. Retreat of the cold halocline layer in the Arctic Ocean. Journal of Geophysical Research-Oceans 103, 10419–10435.
Steele, M., Ermold, W., 2004. Salinity trends on the Siberain shelves. Geophysical Research Letters 31, L24308. doi:10.1029/2004GL021302.
Steele, M., Ermold, W., 2007. Steric sea level change in the northern seas. Journal of Climate 20, 403–417.
Steele, M., Morison, J., Ermold, W., Rigor, I., Ortmeyer, M., Shimada, K., 2004. Circulation of summer Pacific halocline water in the Arctic Ocean. Journal of Geophysical Research-Oceans 109, C02027. doi:10.1029/2003JC002009.
Stoner, J.S., Jennings, A., Kristjansdottir, G.B., Dunhill, G., Andrews, J.T., Hardardottir, J., 2007. A paleomagnetic approach toward refining Holocene radiocarbon-based chronologies: paleoceanographic records from the north Iceland (MD99-2269) and east Greenland (MD99-2322) margins. Paleoceanography 22, PA120. doi:10.1029/2006PA001285.
Stoner, J.S., St-Onge, G., 2007. Magnetic stratigraphy in paleoceanography: reversals, excursions, paleointensity and secular variation. In: Hillaire-Marcel, C., de Vernal, A. (Eds.), Proxies in Late Cenozoic Paleoceanography. Elsevier, pp. 99–137.
Stuiver, M., Reimer, P.J., Reimer, R.W., 2005. CALIB 5.0 [WWW program and documentation]. http://calib.qub.ac.uk/calib/2005.
Thompson, D.W.J., Wallace, J.M., 1998. The Arctic Oscillation signature in the wintertime geopotential height and temperature fields. Geophysical Research Letters 25, 1297–1300.
Tremblay, L.B., Mysak, L.A., Dyke, A.S., 1997. Evidence from driftwood records for century-to-millennial scale variations of the high latitude atmospheric circulation during the Holocene. Geophysical Research Letters 24, 2027–2030.
Vare, L.L., Massé, G.M., Gregory, T.R., Smart, C.W., Belt, S.T., 2009. Sea-ice variations in the central Canadian Arctic archipelago during the Holocene. Quaternary Science Reviews 28, 1354–1366.
Vavrus, S., Harrison, S.P., 2003. The impact of sea-ice dynamics on the Arctic climate system. Climate Dynamics 20, 741–757.
Venegas, S.A., Mysak, L.A., 2000. Is there a dominant timescale of natural climate variability in the Arctic? Journal of Climate 13, 3412–3434.
de Vernal, A., 2009. Marine palynology and its use for studying nearshore environments. From deep-sea to coastal zones: methods and techniques for studying paleoenvironments. IOP Conference Series. Earth and Environmental Sciences 5, 012002. doi:10.1088/1755-1307/5/1/012002.
de Vernal, A., Turon, J.-L., Guiot, J., 1994. Dinoflagellate cyst distribution in high latitude environments and quantitative reconstruction of sea-surface temperature, salinity and seasonality. Canadian Journal of Earth Sciences 31, 48–62.
de Vernal, A., Rochon, A., Turon, J.L., Matthiessen, J., 1997. Organic-walled dinoflagellate cysts: palynological tracers of sea-surface conditions in middle to high latitude marine environments. Geobios 30, 905–920.
de Vernal, A., Hillaire-Marcel, C., Turon, J.L., Matthiessen, J., 2000. Reconstruction of sea-surface temperature, salinity, and sea-ice cover in the northern North Atlantic during the last glacial maximum based on dinocyst assemblages. Canadian Journal of Earth Sciences 37, 725–750.
de Vernal, A., Henry, M., Matthiessen, J., Mudie, P.J., Rochon, A., Boessenkool, K.P., Eynaud, F., Grosfjeld, K., Guiot, J., Hamel, D., Harland, R., Head, M.J., Kunz-Pirrung, M., Levac, E., Loucheur, V., Peyron, O., Pospelova, V., Radi, T., Turon, J.L., Voronina, E., 2001. Dinoflagellate cyst assemblages as tracers of sea-surface conditions in the northern North Atlantic, Arctic and sub-Arctic seas: the new 'n = 677' data base and its application for quantitative palaeoceanographic reconstruction. Journal of Quaternary Science 16, 681–698.
de Vernal, A., Eynaud, F., Henry, M., Hillaire-Marcel, C., Londeix, L., Mangin, S., Matthiessen, J., Marret, F., Radi, T., Rochon, A., Solignac, S., Turon, J.L., 2005a. Reconstruction of sea-surface conditions at middle to high latitudes of the Northern Hemisphere during the Last Glacial Maximum (LGM) based on dinoflagellate cyst assemblages. Quaternary Science Reviews 24, 897–924.
de Vernal, A., Hillaire-Marcel, C., Darby, D.A., 2005b. Variability of sea-ice cover in the Chukchi Sea (western Arctic Ocean) during the Holocene. Paleoceanography 20, PA4018. doi:10.1029/2005PA001157.
de Vernal, A., Hillaire-Marcel, C., Solignac, S., Radi, T., Rochon, A., 2008. Reconstructing sea ice conditions in the Arctic and Sub-Arctic prior to human observations. In: DeWeaver, Eric T., Bitz, Cecilia M., Tremblay, L-Bruno (Eds.), Arctic Sea Ice Decline: Observations, Projections, Mechanisms, and Implications. Geophysical Monograph Series 180, ISBN 978-0-87590-445-0, p. 350. doi:10.1029/180GM04.
de Vernal, A., Hillaire-Marcel, C., Rochon, A., Radi, T., Ledu., D., Bonnet, S., 2009. Holocene Variations of Sea-ice Cover and Sea-surface Temperature in the Western Arctic, from the Fram Strait to the ChukchiSea. In: APEX meeting, Copenhagen, p. 85.
de Vernal, A., Hillaire-Marcel, C., 2006. Provincialism in trends and high frequency changes in the northwest North Atlantic during the Holocene. Global and Planetary Change 54, 263–290.
de Vernal, A., Marret, F., 2007. Organic-walled dinoflagellates: tracers of sea-surface conditions. In: Hillaire-Marcel, C., de Vernal, A. (Eds.), Proxies in Late Cenozoic Paleoceanography. Elsevier, pp. 371–408.
Verosub, K.L., Mehringer, P.J., Waterstraat, P., 1986. Holocene secular variation in Western North America: paleomagnetic record from Fish Lake, Harney County, Oregon. Journal of Geophysical Research 91, 3609–3624.
Versteegh, G.J.M., Blokker, P., 2004. Resistant Macromolecules of Extant and Fossil Microalgae. Blackwell Publishing, Asia, pp. 325–339.
Voronina, E., Polyak, L., De Vernal, A., Peyron, O., 2001. Holocene variations of sea-surface conditions in the southeastern Barents Sea, reconstructed from dinoflagellate cyst assemblages. Journal of Quaternary Science 16, 717–726.
Wolfe, A.P., 2002. Climate modulates the acidity of Arctic lakes on millennial time scales. Geology 30, 215–218.
Woodgate, R.A., Fahrbach, E., Rohardt, G., 1999. Structure and transport of the East Greenland Current at 75°N from moored current meters. Journal of Geophysical Research 104, 18059–18072.
Zabenskie, S., Gajewski, K., 2007. Post-glacial climatic change on boothia peninsula, Nunavut, Canada. Quaternary Research 68, 261–270.
Zreda, M., England, J., Phillips, F., Elmore, D., Sharma, P., 1999. Unblocking of the Nares Strait by Greenland and Ellesmere ice-sheet retreat 10,000 years ago. Nature 398, 139–142.
Zweng, M.M., Munchow, A., 2006. Warming and freshening of Baffin Bay, 1916–2003. Journal of Geophysical Research 111, C07016. doi:10.1029/2005JC003093.